MONITORING THE GULF STREAM: AN APPLICATION OF REMOTE SENSING AND GEOGRAPHIC INFORMATION SYSTEMS

BY MICHAEL F. CROWLEY

A Thesis submitted to the

Graduate School - New Bruswick

Rutgers, The State University of New Jersey

in partial fulfillment of the requirements

for the degree of

Master of Science

Graduate Program in Geography

Written under the direction of

Professor Scott M. Glenn

and approved by

_____

_____

_____

New Brunswick, New Jersey

May, 1993

ABSTRACT OF THE THESIS

Monitoring the Gulf Stream: An Application of Remote Sensing and Geographic Information Systems

By: Michael F. Crowley

Thesis Director:

Prof. Scott M. Glenn

A new method of portraying the ocean surface has been applied to the Gulf Stream Meander and Ring Region. The GRASS Geographic Information System (GIS) was used to create accurate weekly surface maps of the Gulf Stream's north wall and ring locations using a combined remote sensing and in situ database assembled for this project. The database includes AVHRR imagery calibrated for sea surface temperature, Geosat altimeter measurements of sea surface height, and expendable bathythermograph (XBT) measurements of subsurface temperatures. The weekly surface maps created during data rich periods are ultimately used to test and improve dynamical ocean forecast models. The use of a GIS to overlay and interpret the multiple platform database aids in creating more accurate maps than in previous studies of the same time period by NOAA and Harvard University. The development of a new AVHRR compositing technique further increases accuracy by eliminating the feature smearing experienced with the more common warmest pixel composite technique.

The GIS is also used to statistically compare the Gulf Stream locations obtained with the three data sets. The AVHRR-derived surface north wall is 13.2 +/- 14.8 kilometers north of the Geosat-derived maximum velocity axis. The XBT - derived subsurface north wall is 8.9 +/- 11.2 kilometers to the north of the Geosat

maximum velocity axis. Average offsets and RMS values between the axis and north wall increase as one moves from meander trough, to a flat Stream, and on to a meander crest. This demonstrates that the Gulf Stream width increases with increasing anticyclonic curvature, confirming the expected effects of centripetal acceleration on the flow.

Acknowledgements

I wish to express my deepest appreciation to my mentor and friend, Dr. Scott Glenn, without whose knowledge, patience, guidance and support, completion of this thesis would not have been possible. Also, I wish to express my sincerest thanks to another teacher and friend, Dr. Scott Madry, without whose suggestion, I would not have begun the marathon endeavor known as graduate school. I would also like to thank the many organizations and people who supplied me with the data on which this thesis based its conclusions, and provided the support necessary to keep the research going, including: the Institute for Naval Oceanography at Stennis Space Center and the Institute of Marine and Coastal Sciences (IMCS) at Rutgers University for providing all of the financial support; NOAA for providing one set of AVHRR imagery and NORDA for acquiring and rectifying a second set of imagery; Dr. David Porter at the Johns Hopkins Applied Physics Laboratory for providing the Geosat altimeter data; Harvard University, the University of Rhode Island, the Institute for Naval Oceanography and NAVO for providing XBT data; Dr. Norbert Psuty of IMCS for his encouragement, guidance, and careful editing; and especially everyone at the Institute of Marine and Coastal Sciences and the Cook College Remote Sensing Center for providing the computer hardware, software, and support necessary for completing the thesis. I especially would like to extend my gratitude to John Wiggins of IMCS and Jim Gasprich of CCRSC for their constant technical support during the many times it was asked of them. Finally, I want to thank my wife Donna, who saw me through all the frustrations and times of stress with humor, good advice, and her friendship.

Table of Contents

List of Tables

List of Illustrations

Chapter 1

Introduction

1.1 Purpose

Surface mapping of ocean currents and forecasts initialized from those maps, unlike atmospheric weather mapping and forecasting, are in their early stages of development. Previous mapping projects used only single sensors, or did not overlay and analyze multiple sensors in a spatially accurate georeferenced database. The first question addressed by this thesis is: Can ocean mapping be improved using multiple platform remote sensing and in situ data in the georeferenced environment of a Geographic Information System? The test will be performed in the data rich Gulf Stream Meander and Ring Region due to the availability of raw data, the availability of previous analyses, and the high scientific, government and military interest in the region. Gulf Stream maps created here will be qualitatively and quantitatively compared to previous analyses as a measure of the improvement.

The second question that will be addressed is: What is the relation between the Gulf Stream north wall and axis locations as determined by the different remote sensing and in situ data sets? These data sets include Advanced Very High Resolution Radiometer images of sea surface temperature, Geosat altimeter measurements of sea surface height, and expendable bathythermograph measurements of subsurface temperature. Previous investigations have concentrated on comparing the surface and subsurface thermal structure of the Gulf Stream only. With the addition of the Geosat altimeter data, the relationship of the Gulf Stream velocity structure to the thermal can be explored for the first time.

1.2 Early Identification of the Gulf Stream

The Gulf Stream's location has been important to man since explorers first came to the new world. In 1513, the Gulf Stream was first described by Ponce de Leon as he sailed from Puerto Rico to Cape Canaveral. "The current was so swift that his three ships were frequently unable to stem it" (Stommel, 1965). Soon after, some of de Leon's fellow Spanish sailors noticed that there were marked differences in the time it took to travel from east to west and vice versa, in the Gulf Stream region of the north Atlantic. "By 1519 the Gulf Stream was so well known that Spanish ships bound for America came by way of the Equatorial Current but, on their return, passed through the Florida Straits, followed the Gulf Stream to about the latitude of Cape Hatteras, and then sailed eastward to Spain" (Stommel, 1965).

During the 1770's, Benjamin Franklin "was consulted as to why mail packets sailing from Falmouth, England to New York were taking weeks longer than merchant ships traveling from London to Rhode Island" (Stommel, 1965). Franklin referred the question to Nantucket sea captain Timothy Folger, who was familiar with the current because of its effects on whaling. Whales avoid the warm water of the Gulf Stream but ride its northern edge. Folger mapped the Gulf Stream for Franklin, who then realized that the current was latitudinally low enough and physically strong enough to hinder the progress of ships to New York, but was not latitudinally high enough to slow ships traveling to Rhode Island. Franklin ultimately used this knowledge to quicken the transport of French-made weapons to the Colonies during the Revolutionary War.

1.3 Gulf Stream Location and Variability

Today, much more is known about the Gulf Stream's location, movements, structure and dynamics. The gyres of the North Atlantic and Pacific are driven by the anticyclonic, almost circular wind fields that flow over these ocean basins. The intense currents on the western sides of these gyres are caused by the variation of the Coriolis force with latitude (Stommel, 1965). The Gulf Stream is the intense western boundary current of the mid-latitude, anticyclonic, North Atlantic Gyre. The Gulf Stream begins at the Straits of Florida and follows the eastern coast of the United States north to Cape Hatteras (Figure 1). At the Cape, the Gulf Stream turns away from the coast, and flows east-north-east toward the Grand Banks of Newfoundland, where it splits into the North Atlantic Drift to the north and eventually the broad Canary Current to the south. The Canary Current turns south, and then back to the west as the broad North Equatorial Current. The North Equatorial Current splits at the Greater Antilles, with a small flow continuing northwest and meeting with the Gulf Stream at the Straits of Florida. The remainder, and majority of the current mass continues westward, south of the Greater Antilles, then flows northward into the Gulf of Mexico, where it becomes the Loop Current. The North Atlantic Gyre is completed when the Loop Current flows through the Straits of Florida to become the Gulf Stream.

Along the coast of the U.S., the Gulf Stream maintains a relatively smooth flow following the topography (bathymetry) until it reaches Cape Hatteras. It is typical of a western boundary current here, in that it is fast, intense, deep and narrow (Bearman, 1989). These four factors make the Gulf Stream particularly well defined, with a dramatic northern boundary that separates the warm Sargasso Sea water to the south from the cold slope water to the north. When the Gulf Stream turns into deeper water away from the coast and the continental shelf at Cape Hatteras, it begins to meander, almost mimicking a sine wave in places, forming meander crests (peak of

the sine wave) and meander troughs (bottom of the sine wave). Meanders grow in amplitude as they propagate downstream to the east. The meanders can grow so large that they split off as warm core rings to the north or cold core rings to the south. The rings propagate back to the west until they are reabsorbed by another meander. This constantly changing internal ocean weather is not unlike atmospheric weather cell systems. Meanders of the Jet Stream result in warm or cold temperature anomalies, causing high pressure ridges and low pressure storms. Rings spin off the Gulf Stream both to the north and to the south, and are the cause for either warm water anomalies in the north Atlantic slope waters, or cold water anomalies in the warm Sargasso Sea to the south. Future discussion of the Gulf Stream will focus on the dynamic area between Cape Hatteras and the Grand Banks of Newfoundland, the so called Gulf Stream Meander and Ring Region.

1.4 Ocean Current Forecasting

The Gulf Stream's rings and meanders are of interest to many environmental, industrial, private and military groups. At any given time, any one of these groups may want to know what the Gulf Stream's configuration is, and what the future movements will be. In short, these groups would like to be able to map the surface features of the Gulf Stream, and eventually feed these two-dimensional surface maps into the three-dimensional dynamic models that forecast the Gulf Stream's movements, much like meteorologists use computer models to forecast atmospheric weather. Unfortunately, oceanic weather forecasting is much less advanced than atmospheric weather forecasting, primarily because of a lack of data. The total number of in situ measurements taken for atmospheric weather in a few days approximately equals the total amount ever taken for oceanic weather. When oceanographic data exist in large amounts, they are usually either for an isolated time

period or for a geographically-isolated area. However, the dynamic weather fronts in the ocean move much slower than atmospheric weather fronts. Gulf Stream meanders and rings move 15 kilometers a **day** (Lee and Cornillion, 1991), whereas atmospheric weather fronts move many kilometers per **hour**. Therefore, even if the time resolution of clear data over the ocean is not good in comparison to the time resolution of atmospheric weather data, ocean data can often be composited over a few days to monitor the more slowly evolving ocean. These slower movements make surface monitoring of the Gulf Stream Meander and Ring Region possible.

1.5 Geographic Information Systems and Mapping the Gulf Stream

Monitoring, or surface mapping, of the Gulf Stream has been performed in past studies in different ways (Auer, 1980; Robinson et al., 1989). This thesis will introduce new methods of mapping the surface of the Gulf Stream more accurately than in these past studies through the analysis of multiple satellite and in situ data on a Geographic Information System (GIS). A GIS is a computer-based system that is "used to store and manipulate geographic information" (Aronoff, 1989). There are four basic capabilities that a GIS must have (Figure 2). They are (Aronoff, 1989):

1) Data Input
2) Data Management (data storage and retrieval)
3) Data Manipulation and Analysis
4) Output (either tabular or map form)

A GIS is distinguished from other software systems such as CADD (Computer Aided Design and Drafting) and DBMS (Data Base Management Systems) by its ability to integrate georeferenced data (Aronoff, 1989). The GRASS (Geographic Resource Analysis Support System) (U.S. Army Corps of Engineers, 1991) GIS was chosen because of its ability to integrate point, line and raster data, all three of which

are an integral part of the Gulf Stream mapping analysis. Also, GRASS is public domain software, which makes editing, adding and customization of analysis modules in the software possible when necessary for specific analyses. Other GIS packages (e.g., Arc Info, IDRISI) did not have either of these capabilities when the mapping work was begun.

In previous modeling efforts, either one data type was used, such as infrared imagery (Auer, 1980), or, when multiple data types were used, they were compared visually on paper (Robinson et al., 1989). The GRASS GIS permits accurate overlay analysis of multiple data types in a spatially accurate digital database. Quantitative and qualitative comparisons are made to the previous work, but the qualitative analysis and discussions will emphasize the improvements that a GIS lends to mapping surface features. A new image compositing technique is also introduced that is qualitatively compared to the "warmest pixel compositing technique" commonly used in image compositing. The new technique does not spatially smear features as does the traditional warmest pixel approach.

Along with the new monitoring techniques, comparisons are made among the Advanced Very High Resolution Radiometer (AVHRR), Geosat and XBT data used in the mapping process. AVHRR imagery calibrated for sea surface temperature portrays the surface location of the Gulf Stream north wall. Geosat altimeter data are sea surface heights that can be used to define the Gulf Stream's maximum velocity axis (center) at the surface. Expendable Bathythermograph (XBT) data provide estimates of the Gulf Stream's subsurface north wall location at a 200 meter depth. By comparing the north wall location estimates from the three data types, values of the average vector offsets and vector offsets in different dynamic situations are attained. Future mappers can use this information when interpolation of north wall locations are necessary due to missing data.

1.6 Ocean Map and Forecast Applications

In addition to the scientific questions that are answered, there are multiple practical uses for Gulf Stream frontal analyses and the subsequent forecasts made from the frontal analyses. The project partially supporting this thesis was initiated by the Institute for Naval Oceanography (INO) at the NASA Stennis Space Center in Mississippi. This Navy group was charged with the job of improving dynamical forecast models of the Gulf Stream and its rings. The eventual application was to improve submarine operations. At the Gulf Stream's northern wall (the border between the northern edge of the Gulf Stream and the southern edge of the Atlantic slope waters) and at ring edges, there are extreme thermal gradients reaching down to 2,000 meters below the surface. In these areas, ocean temperatures vary horizontally as much as 10^{o}C within 100 kilometers. These thermal gradients cause sonar pulses passing through the area to bend abnormally, missing entire volumes of water. If a submarine were to station itself in an area where the sonar waves do not reach due to this thermal refraction, Navy surface ships would not be aware of the submarine's presence based on sonar reports. With a knowledge of the locations of the Gulf Stream and its rings, Navy surface ships could determine the location of these "blind spots". They could then alter their ship positions to view the entire underwater region, thereby eliminating the "blind spots" (Mooers et al., 1986).

Economic savings are another reason to accurately map and forecast the Gulf Stream. The Gulf Stream is as important for trans-Atlantic ocean transportation now as it was in Ponce de Leon's and Benjamin Franklin's time. Knowledge of the exact locations of the Gulf Stream and its rings can help ships travel faster across the Atlantic and along the East Coast of the United States. Also, oil companies must know current and ring locations for dynamically-positioned drill ships, and for the

new compliant deep water production platforms. Ring movements can drive a drill ship off station, or cause movements in compliant platforms that could be devastating to the oil rig equipment, resulting in expensive downtime and potential environmental damage.

Gulf Stream models and forecasts can also be used to further biological research. The National Marine Fisheries Service uses Gulf Stream positions to determine the locations of many fish species. The temperature differences in the Gulf Stream act as barriers to certain fish species. Fisherman rely on real time maps of the Gulf Stream and its rings to locate potential fishing spots.

Climate models also will be able to use the accumulated data from the maps of the Gulf Stream. A weekly data set that is created when mapping the Gulf Stream contains sea surface heights and sea surface temperatures. If compiled over a series of decades, these data could provide an archive of the reactions of the Gulf Stream to global warming. The Gulf Stream is a vital part of the world ocean circulation known as the Thermohaline Conveyor Belt. Modification of or destruction of this belt could be devastating to future climates because the transport of heat to the polar regions by the Gulf Stream could stop, resulting in extreme heating at the equator and greater cooling at the poles (Bearman, 1989).

One final use of these forecasts is to create a test bed for future satellite development. Through the surface mapping process, determinations on the importance of each data type for mapping the ocean surface and refinements of existing methods of acquiring data can be made.

Chapter 2
History of Modeling and Forecasting

2.1 1940 - 1986

Though the first real time Gulf Stream forecasting effort was begun in 1986 at Harvard University (Robinson et al., 1987a), the concept of Gulf Stream modeling and forecasting was developed long before. With the introduction of submarine warfare and SONAR in the 1940's, many Navy commanders became interested in current movements. Through the 1940's to the 1970's, many groups, both private and government, were working on three-dimensional models of the ocean currents for naval purposes. The Gulf Stream was of particular interest because of its geographic location (i.e., off the coast of the northeast megalopolis of the United States). Its structure was also of interest because it possessed intense thermal and salinity gradients at the north wall and along the edges of warm and cold rings. "Although the width of the Gulf Stream is on the order of 80 kilometers, the strong horizontal thermal and salinity gradients marking boundaries between water masses typically occur within an even narrower 10 - 20 kilometer band" (Glenn and Robinson, 1991). Because of this "band", there exist areas that are difficult to completely view with acoustic soundings (SONAR). Submarines can remain virtually undetected by SONAR in these areas (Cressy, 1986).

In 1981 the U. S. Navy felt it was time to organize the many groups working on ocean models into one, and the first Ocean Prediction Workshop was held in Monterey, California (Mooers et al., 1986). The technology did not exist to begin computer forecasting, but plans were made by the Navy to further focus this group of scientists, creating a new naval organization that would only work on ocean current

modeling and forecasting. Plans were also made to meet in five more years when the computer technology to do forecasting would hopefully be available.

In October of 1985, the Navy created the Institute for Naval Oceanography (INO). Their primary goal was "to conduct a focused and integrated R & D program, directed toward achieving an ocean forecasting capability that will significantly improve support to naval warfare mission and weapon systems" (Onorati, 1986). With an ocean forecasting capability, the Navy would know where to "hide" submarines on a day-to-day basis, and where to look for Soviet submarines. The INO decided to begin ocean prediction testing in the Gulf Stream region.

In 1986, the INO reorganized the major private and government organizations working on ocean forecasting. A second, and more successful, Ocean Prediction Workshop was held during April of 1986. The major purposes of this workshop were "to assess the status of ocean prediction science, to review the latest description of the Navy's needs, and, combining these, to make firm recommendations on how to achieve the stated goals" (Mooers et al., 1986). To make their goals and ideas easily understandable to each other and outsiders, the group separated the process of ocean forecasting into three parts. The overall system was called the Optimal Estimation System and was comprised of:

1) Observational System - system in which both satellite and in situ data were used to map the surface features of the ocean.
2) Dynamical Modeling - this included both three-dimensional fields created from the surface maps, and the forecast models that were run from the three-dimensional fields.
3) Statistical Analyses - these were error estimations of several kinds that are were applied to the model outcomes.

A similar separation concept is still being used today.

2.2 The Harvard University Forecast Scheme (1986 - 1988)

While the Navy was defining the forecast scheme in 1986, Harvard University was actually performing the first complete forecasts. The Harvard Oceanography group was headed by Allan R. Robinson. The forecast project was termed GULFCAST, and the forecast model was called the Harvard Open Ocean Model. The project included forecasts initialized with a series of Nowcasts. Nowcasts are estimations of present ocean current patterns based on previous forecasts and new data (Robinson et al., 1987a). The entire process required 19 steps, the highlights of which will be covered here. The process is extremely important because the Harvard University project was the first of its kind and is the basis of today's modeling and forecasting process. Detailed explanations of the Geosat altimeter, AVHRR and XBT data used in the modeling and forecast scheme are presented in section 2.4.

The first step in the forecast scheme was to acquire AVHRR images calibrated for sea surface temperature during a given time period. These infrared images revealed the locations of important features such as rings, meander crests, and meander troughs. From a series of these infrared images, surface maps were made of the Gulf Stream's north wall and rings. Estimated propagation speeds of the rings, meander crests, and troughs were projected to provide boundary conditions. A "central forecast" was then run for 1-2 weeks from the Nowcast day. XBTs were then dropped in locations where the infrared images were obscured by clouds in order to fill in holes or gaps in the AVHRR imagery, or they were dropped in highly critical areas as defined by the central forecast.

The next step was to perform "sensitivity studies" with slightly modified Nowcasts. These studies determined which of the different model runs best accounted for accurate meander developments, ring formations, and ring absorbtions. The best

Nowcast of those tested was selected to redo the forecast. This time, however, the Nowcast was updated with XBT temperature data to more fully complete the input to the model. To evaluate this second series of forecasts, final XBT flights were flown and new infrared images of days within the prediction time were acquired and the surface features mapped. The surface maps of the true locations were then compared to the forecast model results (Robinson et al., 1987a; Glenn et al., 1987).

Soon after the initiation of the Harvard GULFCAST Project, a new data set became available. Geosat radar altimeter data were made available to the public in 1986. This altimeter measured sea surface height, and could be used to locate the Gulf Stream's north wall and rings, all of which have definite height anomalies (Calman, 1987; McConthay and Kilgus, 1987; Robinson et al., 1987b; MacArthur et al., 1987; Lybanon and Crout, 1987). The altimeter data were soon incorporated into the real time surface mapping at Harvard, and are still being used for historical surface mapping projects.

In 1988, a second forecast model was constructed at the Naval Oceanographic and Atmospheric Research Laboratory (NOARL). With two mathematically-different forecast models, the scientists now had the ability to compare and contrast modeling techniques in order to find the positive and negative aspects of each (Glenn et al., 1991b). Each of the two models was altered following the comparison, and both are still under constant change. Since the completion of the 1988 comparison, new modeling groups have been added to the INO Gulf Stream Forecasting project. They were all tested in 1992 in the Data Assimilation and Model Evaluation Experiment (DAMEE) project.

2.3 1991 - 1992 -- DAMEE and the Modern Forecast Scheme

The Institute for Naval Oceanography sponsored the DAMEE (Data Assimilation and Model Evaluation Experiments) project in 1991 and 1992, which provided partial funding for this thesis research. The following is a brief summary of this project and the current forecast scheme.

The DAMEE project has redefined the ocean forecasting scheme into four components. These components are:

1) An Observation Network to view and define the ocean surface.
2) Statistical Models to project the surface maps onto a three-dimensional grid.
3) Three-dimensional Forecast Models.
4) A Data Assimilation Scheme linking the first three components together.

Use of an accurate Observation Network to map the ocean surface is a vitally important step in the forecasting process, because all other steps rely on the data created during this first step. Rutgers was charged by the DAMEE group to create the surface maps for the experiments. In this case, it involved defining the surface features of the Gulf Stream based on available remotely sensed and in situ data. These data currently include satellite thermal infrared imagery from the AVHRR satellite, satellite altimeter measurements from Geosat, and in situ temperature measurements from expendable bathythermographs (XBTs). The XBT data were from multiple sources, including ship and aircraft deployments. Improvements to the observational network and analysis of the data for surface mapping are the focus of Chapters 4 and 5.

After accurate maps of the Gulf Stream surface were produced, statistical models were used to produce three-dimensional versions of environmental fields for the Gulf Stream and its rings. The INO used a program called "OTIS" (Ocean Thermal Interpolation System) (Clancy et al., 1990) to create these three-dimensional

fields of the Gulf Stream's velocity, density, salinity and temperature, based on the two-dimensional surface maps created at Rutgers.

Dynamic forecast models used the three-dimensional output from OTIS as the starting point for short term predictions of the position of the Gulf Stream and its rings. The DAMEE project's ultimate goal was to see which of four selected forecast models is the most accurate for forecasting. This has not yet been determined. These models are listed here by name, project leader, and organization (DAMEE, 1991):

1) FLEXCAST - Allan R. Robinson, Harvard University.
2) DART - Dan Fox, INO.
3) PEDAM - George Mellor, Princeton University.
4) SPEM - Dale Haidvogel, Rutgers University

The forecast predictions by these models generally range from one day to a few weeks. If accurate surface maps are made on a weekly basis for a month, the forecast models can be run using the first week's map, and then error checked against the true location on a weekly basis for the remainder of the month. This run and check of the forecast models allows the modelers to see where and when problems occur. Simply, the more sequenced surface models created in step 1, the more chances there are for the forecast modelers to identify where the forecast model begins to diverge from the observations.

The fourth component, Data Assimilation, is an integration of the three components previously discussed. Data assimilation in oceanographic models is in its infancy and is an active area of current research. Forecast model data assimilation schemes initially required full three-dimensional fields for assimilation, rather than individual data sets. As an example of the early assimilation process, steps one to three (data observation, statistical modeling, forecast modeling) are run in order. After the dynamic model has been run for several days, the modeler assimilates the three-dimensional fields generated from the next surface model (map) and restarts the

forecast model run. This input of new and correct data on an approximately weekly basis adjusts the model's forecasts to keep them on track. Eventually, this assimilation will be done on a daily basis, with individual partial data sets rather than with full 3-D fields. The daily assimilation will be difficult, however, because on any given day only partial areas of the Gulf Stream are observed.

As should be apparent, the observation and mapping step is very important. The Gulf Stream cannot help but follow the rules of physics. There are physical reasons for all of its meander and ring movements. If the maps created in step 1 are inaccurate, then in step 4 modelers may be correcting their models to predict events that are physically incorrect. In these cases, the models would be altered improperly, even though the forecast modelers feel they are upgrading the model. This is one reason an accurate observational network and surface mapping scheme are so important.

2.4 The Observational Network -- Geosat, AVHRR and XBT Data

Correct interpretation of raw satellite and in situ data is perhaps the most important component of ocean forecasting because all other steps use the data as their input. Throughout this thesis, there have been references to different types of data. The three used in this project are Geosat altimetry data, AVHRR imagery, and XBT temperature profiles. Detailed explanations of each data type are given here.

2.4.1 The Geosat Altimeter

The Geosat satellite was launched on March 12, 1985 and ran through January, 1990. The primary mission (labeled the Geodetic Mission) was "to provide the dense global grid of altimeter data required to improve the determination of the earth's gravitational field" (McConthay and Kilgus, 1987). The secondary mission (labeled

the Exact Repeat Mission) was "to detect mesoscale oceanographic features in a timely manner" (McConthay and Kilgus, 1987). The altimeter flew at an 800 kilometer altitude. After the Navy's primary goal was achieved in September of 1986, Geosat was put into a 17-day exact repeat orbit. The antenna of the Geosat radar altimeter was aimed at nadir (straight down) and fired a pulse at a frequency of 13.5 gigahertz every 980 microseconds (MacArthur et al., 1987). The time interval between beam transmissions translated to one height measurement every 0.67 kilometers on the ground (Porter et al., 1989). Every 10 samples were averaged, resulting in one sample every 6.7 kilometers on the ground. The pulse measured the distance from the satellite to the ocean surface to within 3 centimeters. The 17-day repeat orbit resulted in a sampling distribution pattern like that in Figure 3a. Each repeat orbit was required to be within 1 kilometer of the nominal orbital path. Sea surface heights are only recorded directly below the satellite.

The distance from the satellite to the ocean surface is not sufficient for interpretation of sea surface height. Satellite orbital error correction is necessary, and a geoid must be used as a base from which to measure. The geoid is the gravitational equipotential surface to which the sea surface would relax if all internal motions in the ocean were to cease (Porter et al., 1989). Once these corrections are completed, the sea surface height associated with ocean currents can be analyzed. Sea surface height differentials in the Gulf Stream Meander and Ring Region are typically on the order of 1 meter relative to the geoid, whereas variations in the geoid are on the order of 100 meters. Figure 3b illustrates data from an ascending Geosat track (satellite is moving from southeast to northwest). The ground track is the projection of the orbit on the earth's surface and is represented by the straight line. Also for analysis, this straight line is considered to represent the local geoid. The sea surface topography is plotted perpendicular to the ground track (or geoid), with positive to the right and

negative to the left. These maximum height offsets are approximately +/- 60 centimeters. The point where the sea surface topography crosses the geoid is the location of the Gulf Stream's axis. In Figure 3b, the Gulf Stream's maximum velocity axis is located at approximately 38ºN, and a cold ring is centered at about 36.5ºN. The north wall is located approximately 20 to 30 kilometers to north of the axis. The OTIS three-dimensional statistical model can use either the axis or the north wall, plus ring locations, for the major input. In the DAMEE project, the north wall was used.

There are two major operational constraints with the Geosat altimeter. First, even with corrections, the root mean square error of the sea surface heights derived with the best available geoid is 9.6 centimeters (Glenn et al., 1991a). This vertical error potentially can translate into a horizontal error of 10 kilometers on the positioning of the Gulf Stream and the rings at the earth's surface. Secondly, Geosat only repeats its orbit once every 17 days. Therefore, the temporal resolution of the data is intermittent when compared to other satellites, such as AVHRR.

2.4.2 The Advanced Very High Resolution Radiometer

The Advanced Very High Resolution Radiometer (AVHRR) has been operational on NOAA polar orbiting satellites for more than a decade. Though its resolution is no longer considered high, the data acquired are of sufficient resolution to find large scale ocean features. Presently, there are four operational AVHRR satellites, each maintaining orbits of 850 kilometers. "Each satellite orbits the earth 14 times daily and acquires complete global coverage every 24 hours" (Sabins, 1987). This cross-track multispectral scanner "acquires images with a width of 2700 kilometers and a ground resolution cell of 1.1 kilometers" at nadir (Sabins, 1987). The satellites have five bands, each focusing on different wavelengths ranging from visible to thermal (0.62, 0.91, 3.7, 10.8, and 12.0 micrometers). To view oceanic

surface features that are highlighted by thermal gradients, bands 4 and 5 (10.8 and 12.0 micrometers respectively) are combined and converted to images of sea surface temperature. All of the images used in the DAMEE project were geocorrected and converted to sea surface temperature by NORDA, and look similar to Figure 4. These images had a pixel resolution of 2.25 kilometers and were accurately georeferenced to within 1 pixel in any direction. Spatial error in any image could therefore be 2.25 kilometers. Red colors in Figure 4 are about 20^{o}C whereas dark blue areas are cooler water (10^{o}C). The large gray areas are cloud cover. The meandering Gulf Stream is the obvious red and orange feature running horizontally across the image. The Gulf Stream north wall is defined as the location of the largest thermal gradient. In the case of multiple large gradients, the most southerly is chosen (Horton, 1986).

The major setback with AVHRR imagery is that it cannot penetrate clouds. In figure 4, not only are the gray areas clouds, but the green and blue areas to the south are the remnants of thin clouds which allowed some energy to pass through to the satellite. Geosat is not affected by clouds, however, and the combination of these two can prove very useful, especially if there are Geosat tracks in areas where there are cloud effects on an AVHRR image. XBT data also have this ability to fill data gaps in imagery.

2.4.3 Expendable Bathythermographs

Expendable bathythermographs (XBTs) are simply thermometers dropped from either planes or ships, which continuously relay temperatures back to the surface source as the XBT drops to the ocean floor. They generally reach depths of a few hundred meters before their communication wire with the surface breaks. The XBT data used for DAMEE came from four sources: Harvard, INO, the University of Rhode Island and NAVOCEANO. The geographic coordinates of each XBT are

saved by either the aircraft navigation system or boat navigation system, and any error in the geographic coordinates are specific to each XBT survey. For example, the inertial navigation systems on operational Navy flights are usually accurate to within 5 kilometers, whereas the navigation systems on the Navy research aircraft underflying Geosat tracks are more accurate. At a 200 meter depth in the Gulf Stream Meander and Ring region, the 15^{o}C isotherm is well recognized as the separation point between the Gulf Stream's north wall and cooler North Atlantic slope water. (Cornillion and Watts, 1987; Mitchell and Dastugue, 1990). Knowing this, one can locate the Gulf Stream and its rings based on XBT data. A sample distribution of XBTs is shown in Figure 5, with temperatures plotted next to each point in degrees Celsius.

The surface expression of the Gulf Stream north wall can shift up to 15 kilometers north or south of the more stable subsurface north wall location determined from XBTs (Cornillion and Watts, 1987). Also, there is an "ocean skin effect" during the summer months. This effect is where the entire surface layer of the ocean is warmed to a relatively similar temperature by solar heating, hiding the surface thermal features of the ocean (Hepplewhite, 1989). AVHRR's usefulness is limited when this ocean skin effect occurs because AVHRR only measures the temperature of the top few micrometers of water, but XBTs can measure below this. Geosat measures height, which is not affected by solar heating. Combining all three data sets thus can reduce error, and help to make accurate two-dimensional surface maps of the Gulf Stream and its rings.

Chapter 3

The DAMEE Project

3.1 Requirements and Surface Mapping

The requests from the DAMEE project leaders at the Institute for Naval Oceanography (INO) for the Rutgers University surface mapping group were:

1) Compile a set of approximately weekly spaced Gulf Stream north wall locations for a 1.5 month time period, in the geographic region defined by latitude 34^{o}N north to 45^{o}N, and longitude 50^{o}W westward to 75^{o}W.
2) Compile a set of warm and cold ring locations for the same days as the north wall locations. In addition, provide an estimate of the rings' average radii and swirl velocities.

With these two sets of data, the forecast modelers would be able to test the dynamical forecast models on a weekly basis with accurate data, which was the ultimate goal of the project. To realize these two requests, a multistep procedure of image and data processing, data integration, and data analysis was implemented using the GRASS GIS.

The first step was to choose the time period to model. The years of 1987 and 1988 had the most extensive and most diverse yearly data sets. With recent and planned launches of additional oceanographic satellites, future data sets are expected to be of the same type and as large or larger than the 1987 and 1988 data set. Consequently, these two years were chosen to test forecasting feasibility and ease because they would be an excellent way to determine if Gulf Stream forecasting and possibly global ocean forecasts will be feasible in the future. In order to focus on exact dates, cloud-free AVHRR imagery was necessary. This imagery could provide the most complete view across the Gulf Stream meander and ring region when clouds

were not present. In comparison, Geosat data are simply linear samples and the XBT data are simply, for surface modeling purposes, site samples. The imagery can cover the entire geographic area, although about 70% cloud free is the clearest coverage. Using GRASS, a simple time series movie was created of all the imagery during those two years. By viewing this time series, it was clear that the time periods of June and September, 1988 were the least cloudy 1.5 month periods. June was selected because it lacked the "ocean skin effect" that was so prevalent in September. The September imagery was clear, but it was very difficult to discern features because of the constant temperature surface, especially in daytime imagery.

After June was chosen as the test case, it was necessary to develop a general understanding of the locations and movements of features (Gulf Stream meanders and rings) during the period. To accomplish this, not only was the imagery viewed, but three 17 day composites of the Geosat data were created (Figures 6,7 and 8). In the Geosat composites, not only are north wall locations evident, but so are warm and cold rings. Some cold rings were never visible in the infrared imagery due to clouds or lack of sea surface temperature contrast. A common problem with cold rings is that they are not viewable in the infrared imagery because the cold water sinks below the surface, and is covered by the warm Sargasso sea water. Figure 7 shows the location of one such ring at 37^{o}N, 54^{o}W. A monthly composite of all XBT data was also created to get a general picture of the period (Figure 9). One striking feature of Figure 9 is the southerly extent of blue and black (cold) XBTs at 61^{o}W. This is the result of an abnormally large trough that will be discussed below. With a general idea of the ring and the north wall's relative locations during this month, it was now necessary to choose the exact days to map.

Based on clarity of imagery, the dates May 25, May 30, June 5, June 13, June 22, June 29 and July 4 were chosen. The dates are anywhere from 5 to 9 days apart.

As stated earlier, any one image is rarely cloud free in more than 70% of the study area. In order to get a mostly solid image across the area, it was necessary to composite images from consecutive days. The slow movement of the meanders permit combinations of images over plus or minus a few days to remove clouds without much distortion of the features over time.

The first new technique that this thesis introduces is the concept of "patching". Previously, the standard image compositing technique used was the warmest pixel composite. A warmest pixel composite is simply a technique whereby a group of images are chosen, and overlaid on a map projection or grid. For each cell in the resulting single image, the maximum temperature (cell value) recorded from the group of images is used. This results in a smearing of true meander and ring shapes because these features move slowly over time. Meander crests will appear wider than they actually are, meander troughs narrower, and rings will appear to have greater average radius. This technique makes for an esthetically pleasing picture, but is not scientifically accurate. The patching technique used on the GRASS GIS requires more work, but does not smear the shape of features.

In patching, a single first image is chosen, based on optimal clarity (cloud free over 50% of the area). In this case, each first image is on the same day as the mapping date. Then, a temperature threshold is set, based on that image, setting all values below a certain temperature to zero. Thresholding eliminates clouds and many cloud effects. It is the simplest cloud removal technique. More sophisticated techniques can be substituted in the future if required. This thresholding is performed on all images within a few days of the center image. All zero values that result in each image are viewed as holes in the data by GRASS, so if one were to overlay two images, the areas of zero data in the top image would appear as a window, and be filled with data from the underlying image. In patching, the center day is the top image, with the images of

+/- 1 day laid directly below, the images of +/- 2 days laid below that, and so on. Eventually the colder temperatures that were originally thresholded out are patched back underneath the threshold image, but only for esthetic purposes (color fill in the upper reaches of the region, away from the Gulf Stream). When patching is completed, an image of values above a certain threshold is output. The resulting patched image does not smear the shapes of features as does the warmest pixel composite.

An excellent example of a warmest pixel smear versus a patched image is Figure 10. The background image is a warmest pixel composite. The black line is the north wall from the patched image and the white line is the north wall as interpreted from the warmest pixel composite. The meander crest from the warmest pixel composite is much wider on the tail ends than that from the patched image. Because the wrong initial shape will cause the dynamic forecast models to forecast the wrong meander evolution, the introduction of patched composites with preserved shapes is a critical advancement in the mapping process.

Once the patched images are complete, the Geosat tracks and XBT locations within +/- 3 days are overlain on the image to create the final maps. Figures 11-17 are the completed maps. Table 1 lists the days (Julian calendar) of the AVHRR images, Geosat tracks, and XBT data used in each map. For each map, the AVHRR image is color-coded, with blue representing approximately 10^{o}C, and red representing temperatures of approximately 25^{o}C. Clouds appear as gray areas throughout the image. Both the Geosat tracks and XBT locations are color-coded by day. Black is on the same day as the center image, violet is +/- 1 day, yellow is +/- 2 days, and white is +/- 3 days from the center day. In addition, the XBT sites are coded by icon. The 15^{o}C isotherm at 200 meters below the surface is the relative location of the Gulf Stream's north wall and warm ring edges (Cornillion and Watts, 1987). Anything less than

15ºC is either a cold ring or shelf water, whereas any water warmer than 15ºC is the Gulf Stream, Sargasso Sea water, or a warm ring. The following icons represent the following temperature ranges at 200 meters:

1) Square: > 17.5ºC
2) Circle: 15 - 17.5ºC
3) Star(*): 12.5 - 15ºC
4) Plus(+): < 12.5ºC

In addition to the AVHRR image, Geosat altimetry, and XBT data, the 200 meter isobath is plotted in white, running southwest to northeast across the top of each map. This is the continental shelf break, which not only confines the Gulf Stream rings to the south, but also is the location of the shelf/slope thermal front, which is clearly observed in the June 5 image. The sea surface temperatures in this area follow the contour of the shelf. The series of thick black lines on each image is the mapped Gulf Stream north wall and ring edge locations. The black "x"s indicate the center of each ring. In some instances, the rings were not visible on the AVHRR image on a given day, and their center locations had to be estimated by Geosat, XBTs or interpolated. These rings' centers appear simply as an "x" in the image.

These final maps were not the only portrayal used to map the north wall and rings. The final north wall maps, the thick black lines on each map, were created in small pieces. The first major consideration when mapping the wall is that the surface thermal signature of the Gulf Stream weakens as if moves from west to east. This dictates that the analysts subjectively change the temperatures at which they separate the north wall from the slope water as they move east. It was therefore necessary to interpret small sections of the images to precisely assess and map the temperature gradients, all easily accomplished using a GIS system.

Multiple enhancements of individual images were also used to create the north wall and ring location maps. In GRASS, an enhancement is created simply by stretching a full color scale (blue-green-yellow-orange-red) across a limited amount of pixel values in an image. For example, Figure 18a is an enlarged view of a single image from day 176 of 1988. This image has the standard color scheme used in the final images. Figure 18b is an enhanced view of the same area, lending color only to temperatures between 20 and 22°C as opposed to the full scale of 5 to 27°C. As is obvious, it much easier to see the meander and ring circulation with the GRASS color enhancement. When digitizing the north wall, these enhanced images, the final images, Geosat tracks and XBT data could all be put on screen at one time, and areas could be enlarged to accurately map small pieces of the wall, one section at a time. The north wall segments were then snapped together and smoothed to create the final black line superimposed on every image.

3.2 May - June 1988: Ring and North Wall Histories

Before a discussion of the Gulf Stream's north wall and ring movements, it is necessary to separate the study area into three regions of varying activity. The first region is located between 75°W and 68°W. This is an area of relative stability and calm with very little movement of the north wall and rarely any ring formation events. It is noted that small perturbations in the Gulf Stream in this area can propagate east, grow into large meanders, and eventually into rings. The second area is located between 68°W and 58°W. This was the area of greatest activity during the study period. Not only were warm and cold rings created and absorbed, but a massive, deep meander trough grew to an amplitude of 460 kilometers. The third area is between

AAS
Comment [1]: Page: 27

58°W and 50°W. This region had only one major event, when a large "S"-shaped meander absorbed a warm ring at the end of the time period.

The first day of the study period was May 25, 1988 (Figure 11). Four warm rings are located to the north of the Gulf Stream, whereas five warm rings are located to the south of the Gulf Stream. Figure 19 shows the ring centers with their labels based on their June 13 locations (note that there are five warm rings). For simplicity, the rings will be referenced as W1 (warm ring 1) and C2 (cold ring 2), etc. Because there are no data before May 25, speculations were not made on ring movements prior to this time. Also, there is relatively little movement in rings W1, C1 and C2 throughout the period, and therefore no discussion will be made on their progress. Table 2 lists the data types that were used to locate the ring centers, whereas Table 3 lists the average speeds and compass directions of the rings between analysis days during the entire one-and-a-half month time period. Table 4 lists the rings' radius, depth, and estimated rotation speed based on the strength of the Geosat altimeter signal. For future reference there is a need to point out two features in the north wall on May 25. The large meander at 67.5°W is in the process of separating into what will become W3 by May 30. The other feature is the initial development of a crest at 66°W. This seemingly insignificant bulge in the north wall eventually becomes a large crest, which both absorbs a ring and forces complex ring movements.

By May 30 (Figure 12), W3 has separated from the north wall at 63°W. The bulge at 65°W and the trough at 66°W have both grown. The trough eventually dissipates into a flat Gulf Stream. At 62°W, a small dip in the trough has begun to form. The final event worth noting on this relatively quiet day is the beginning of a trough formation at 53.5°W. This trough and the attached meander to the east eventually absorb W5.

The bulge at 65°W and trough at 62°W are very obvious by June 5 (Figure 13). The trough has deepened quickly, within a 6 day period, while the bulge has begun to interact with W2. There is a jump in speed from almost 1 to 5 km/day in W2, whereas the direction of the ring changes from south to west-south-west (Table 3) during the next few days. Both of these changes are forced by the northward moving meander. Also, the trough/meander feature at 53°W is increasing in size.

The next analysis day is June 13 (Figure 14), which is 8 days after the previous surface analysis, and reveals a great change in the depth of the trough at 62°W. This once small bulge has now propagated into a large trough/meander feature having major effects on the movements of three rings. This trough has begun to push C3, changing its direction from southwest to southeast and increasing its speed from about 6 km/day to 10 km/day (Table 3). The northwestern meander on this feature pushes W3 to the north, and consequently increases W3's speed from about 1 to 7 km/day (Table 3). The northeastern meander on this feature at 59°W pushed W4 toward the northeast, away from its previous westerly path. In addition, the depth of the small trough at 53°W has increased. This trough has its most dramatic change in structure during the time between the June 13 and June 22 (Figure 15) analyses. This is perhaps due to the length of time between surface analyses (9 days), which is the longest between any of the seven study days.

By June 22, the trough at 53°W has broadened into a large "S"-shaped meander, moving rapidly toward W5, which in turn is moving back toward the meander. The most dominant event of this day is the absorption of C3 by the trough at 61°W. This trough, with the absorbed ring at its base, is over 460 kilometers deep. The meanders at the top of the trough continue to push W3 and W4 to the northeast. W3 has however shrunk dramatically in size, going from an average radius of 104.1 to 75.4 kilometers (Table 4).

The June 29 map (Figure 16) indicates that a quick closing of the trough at 61°W has begun, with the eastern wall of the trough stalling, and the western wall moving towards the east. Robinson et al. (1988) present evidence that this process is the preferred sequence of events for cold ring formation. Both W3 and W4 are now moving abnormally fast (14 and 15 km/day, respectively) due to interactions with the meander peaks on either side of the trough. Speeds of this magnitude are rare for rings, and usually do not last for more than a few days. There is a sudden jump in speed toward the west for both rings C4 and C5 (Table 3). One possible reason for this is the stall and regress toward the west of the elongated trough at 61°W. This trough is quickly closing and weakening, possibly dragging C4 and C5 with it. Finally, W5 has now moved close to the meander at 52°W and will soon merge with it.

The last analysis day is July 4 (Figure 17), 5 days after the previous map. On this final day, W5 no longer exists, having been absorbed by the "S"-meander at 51°W. Whereas this ring was destroyed, C3 has reemerged associated with the collapse of the trough at 61°W. The ring is almost peanut-shaped, due to the elongated trough from which it formed. Now that this trough has dissipated and the Gulf Stream is no longer forcing new water into the area of C4 and C5, these rings have increased their speeds towards the west (Table 3). W3 continues to move in a similarly-induced sprint, but toward the northwest, due to the presence of the meander at 62.5°W. An excellent example of a sprint/stall ring movement due to the Gulf Stream interference is now prevalent in C4. The speed has changed from approximately 15 to 2 km/day in 12 days. The meander at 60°W that was once pushing C4 is no longer within range of the ring and it has stalled.

3.3 Summary

Oceanographic events during the 6-week study period in the Gulf Stream Meander and Ring Region can be summarized by region: western (75°W-68°W), central (68°W-58°W), and eastern (58°W-50°W). There were no events of consequence in the western third. The Gulf Stream remained relatively straight and no rings were formed or absorbed. The central region was the most active. There was a warm ring birth early in the study period. This was followed by the formation of an extremely deep meander trough and a cold ring absorption. The trough eventually separated from the Stream and formed a large cold ring near the end of the study period. In the eastern region, a large "S"-shaped meander slowly evolved, eventually absorbing a warm ring near the end of the study period.

Chapter 4

Comparisons of North Wall Surface Maps to Previous Work

4.1 Introduction

With the completion of the new surface maps, it is now possible to compare these new analyses with maps created for the same time period using previously defined techniques (Auer, 1980; Robinson et al., 1989) and with those created from warmest pixel composites. Only comparisons of the Gulf Stream north wall locations, not ring locations, are considered here. The Clark (1988) study, using the Auer (1980) technique, contain no exact data on ring locations whereas the Robinson (1989) study contained some completely different rings. Qualitative and quantitative comparisons can be made to both the warmest pixel and the Robinson et al. (1989) techniques. These two studies resulted in complete north wall estimations across the entire region from 73^{o}W to 53^{o}W. No averaged quantitative comparisons can be made to the results from the Clark (1988) study because the analysis did not result in a complete north wall across the region. Instead, a hand drawn map of all visible surface features (Figure 20) was produced to which the only quantitative comparison that can be made is maximum offset. Before proceeding further with the comparisons, it is necessary to first discuss how the other studies created their surface maps to highlight the improvements in methodology.

4.2 Previous Methods of Mapping Gulf Stream Surface Features

4.2.1 Warmest Pixel Composites

Warmest pixel composites were created for this study using the same images used to create the patched images for this thesis. The warmest pixel technique is the same as that described in Chapter 2. An unexpected Gulf Stream north wall displacement was realized after comparing north wall locations derived from the

warmest pixel composite with those created for this study. One initially would expect that the north wall derived from a warmest pixel composite would either be located at the same latitude or farther north than a north wall derived from a patched image. This is because the warmest pixel technique saves the highest pixel value from the given set of images, whereas the patching technique uses one image for more than 50% of the final image. If there is any meandering of the warm Gulf Stream to the north over a series of days, the final warmest pixel composite will retain the most northern position. Any movement to the south would simply be masked by warmer values from previous days. Warmest pixel composites thus smear moving Gulf Stream meanders, resulting in crests that are higher and wider and troughs that are shallower and narrower.

This study has revealed that in certain circumstances, warmest pixel composite results can actually be south of those from a patched image composite. An example of this southerly displacement is noted in the May 30 maps. The image from day 151 (Figure 21a) exhibits an obvious Gulf Stream meander location at 38^{o}N, 66^{o}W, but the sea surface temperature signal is weakened by sparse cloud cover. Day 153 (Figure 21b) has a much stronger sea surface temperature signal in the same area, but between the two days, the trough propagated to the east. When a warmest pixel composite is made of these two days, the surface signal strength of day 153 is prevalent over that of day 151 because of a lack of cloud cover. Figure 21c is the warmest pixel composite with the patched north wall (black) and the warmest pixel north wall (red) overlaid on the image. At 38^{o}N, 66^{o}W the subjective analysis of the warmest pixel composite results in a north wall location farther to the southeast because that is the location of the greatest thermal gradient. The warmest pixel composite north wall of this area is actually based on day 153, not day 151. This displacement to the southeast in cloud

effected composites is an error a surface mapper will not be able to distinguish when using a warmest pixel composite.

4.2.2 The NOAA Mapping Technique

The NOAA mapping technique, described by Auer (1980), was used by Clark (1988) to create maps of all surface features in real time during 1988. Auer's (1980) technique is simply to use only AVHRR imagery to map the features every three days. Auer (1980) first uses imagery from the day of preference, draws the surface features over the imagery, then uses images from the previous two days to fill in the cloud gaps. This use of images to fill in the gaps in image data is similar to the patching technique, but computer overlay in a geographically accurate database was not used. Only manual overlays of manually georeferenced maps were used to create the analyses. This is highly inaccurate when the only land features to georeference in the images are in the extreme north west corner of each image (i.e. the northeast coast of the U.S. and Canada). Feature shapes may be preserved, but in the eastern region of each image, large locational offsets due to the lack of registerable features (i.e. land) can occur.

4.2.3 The Harvard Mapping Technique

The final technique that will be compared to this thesis work is that by Robinson et al. (1989), which also was done in real time at Harvard University. The Harvard technique is similar to this work in that Geosat, AVHRR, and XBT data were used. Their analyses also resulted in a complete north wall across the Gulf Stream region, not pieces of north wall like that from the NOAA analyses. One difference at Harvard, however, was that the data were overlaid, compared and mapped on hard copy paper overlays. A second difference is that a geoid was not used in estimating the

north wall location from the Geosat signal. A collinear pass-minus-pass difference technique was used to remove the geoid. A complete discussion of this technique is described in Porter et al. (1989). The collinear pass-minus-pass difference technique is simply a subtraction of the Geosat signal of one pass from the next consecutive pass to arrive at a single signal for the change in sea surface height. This resultant signal will not show an obvious Gulf Stream axis location if the Stream has not had a large latitudinal displacement over the 17 day period between passes, or, if there is a ring near the Gulf Stream. Either of these two events could cause the signal from the collinear pass-minus-pass difference technique to be topographically flat. Interpretation of the collinear pass-minus-pass difference technique also requires knowledge of feature locations in the older pass, which may be imprecise. The geoid subtraction is much more effective in producing a varying topographic signal in these cases because there is only one oceanographic signal, and no smoothing by subtraction of two oceanographic signals (Porter et al., 1990). In addition, Harvard simply determined the Gulf Stream axis location by eye, whereas in this study, the Gulf Stream axis was precisely defined as the location of the maximum slope in the sea surface height.

4.3 Comparisons to Previous Mapping Techniques

Figures 22-28 show the north wall locations derived using the four techniques for each date. Note that the NOAA analysis has had much of the extraneous data that appears in Figure 20 edited out. Only the north wall locations remain. Table 5 shows the maximum distance offsets, defined as the maximum perpendicular distance, of the north walls created using the Harvard, NOAA and warmest pixel techniques, to those resulting from this study. It also shows the average offset of the Harvard and warmest pixel composite techniques to this study. The average offset is defined as the area

between the two lines divided by the average length of the lines. The comparisons were made between 73°W and 53°W because the Harvard results were designed to be accurate in this region.

The improvements of this study's analysis over the warmest pixel composite technique has already been discussed in depth. The reason the warmest pixel average offsets are small is because much of the north wall from the warmest pixel composite is actually the exact same north wall location as found in the patched technique. When creating the warmest pixel north wall, there were occasionally areas where clouds remained over the Gulf Stream even in the final warmest pixel image. Instead of redigitizing a north wall in these cloudy areas, pieces of the north wall derived from the patched analysis were spliced in. During the June time period these cloudy locations were generally in the areas east of 62°W. Table 6 shows offset measurements of the patched analysis to specific sections of the north wall that were strictly from warmest pixel analysis. These sectional comparisons exhibit much larger offsets and better represent the offset that would result from a typical warmest pixel composite analysis over the entire region.

A discussion of the major analyses differences between the north wall locations generated from this study to those from the other three studies will now be given. This author cannot and will not make assumptions as to why the north wall locations from the other studies are located where they are, but will list this study's reasoning for locating the north wall in areas where there are marked offsets from the other studies. There is no methodology to measure the accuracy of the separate techniques, but by using a GIS to incorporate more data in this analysis compared to the previous studies, it is assumed that this study more closely approaches reality.

On May 25 at 73°W and 68°W (Figure 22), enhanced infrared imagery from day 146 confirms the location of the Rutgers north wall. At 52°W however, there is no

imagery to confirm the north wall. Here the north wall was located by a descending Geosat track (Figure 11) from day 144. This is two days before the center image day, but is the only data set in this region.

Figure 23 shows the four May 30 analyses, but the Harvard and NOAA analyses are actually for two days later. The maps are still very much alike, except for the areas east of 62°W. Two Geosat tracks confirm the Rutgers positioning of the Gulf Stream between 62°W and 58°W (Figure 12). Because meanders propagate east, the offset in the north wall location from the Harvard results is very curious, in that the Harvard meander in this area is west of the Rutgers meander. The large ring-shaped meander of the NOAA analysis at 63°W is considered a ring by the Rutgers analysis because of the Geosat track that crosses through that area in Figure 12. Also a single cold water XBT can be seen in Figure 12 at 61°W, 39°N, which indicates a separation of the north wall from this ring.

On June 5, the differences in the NOAA and Harvard analyses from the Rutgers analyses, and the large average north wall offset of the Harvard north wall from the Rutgers north wall (29.2 km.) (Table 5)(Figure 24), is possibly due to the three day interval between the analyses, at least west of 58°W. The eastward offset of the Harvard analysis from the Rutgers analysis on the meander between 63°W and 67°W, and the deepening of the trough at 62°W, could definitely be explained by the three day lag time between analyses because meanders deepen and propagate east with time. Both Geosat tracks and the AVHRR image in the map of June 5 confirm the location of the Rutgers north wall in both of these locations (Figure 13). The large offsets between the NOAA, Rutgers and Harvard analyses east of 57°W is definitely due to a lack of clear imagery, Geosat and XBT data. The north wall locations in these areas are estimations.

Again on June 13 (Figure 25), there is an time interval between the Harvard and NOAA analyses and the Rutgers analysis, but this time only two days (Table 5). The average offset of the Harvard north wall from that of Rutgers is only 12.0 kilometers, the smallest average offset of the entire study period. Even though the analyses are two days apart, the extreme clarity of the AVHRR imagery from June 11 to June 15 made it very easy for all parties to locate the surface features of the Gulf Stream, perhaps negating the differences in analysis techniques. The offsets between analyses west of 56°W could again be explained by the meanders propagating eastward during the two day time lag. The difference between the Rutgers and Harvard analyses at 52°W, however, cannot be explained. The Rutgers north wall location in this area was based on a Geosat track, XBT's and infrared imagery (Figure 14).

Considering some of the extreme dynamic movements of the Gulf Stream like the large trough at 62°W, and the warm ring interactions with the Stream during June 22, the analyses are quite similar (Figure 26). The major difference in the NOAA analysis from that of Rutgers is at 62.5°W, where Rutgers indicates a ring separation and NOAA maintains a large meander. An image enhancement of day 176 indicated that there was at least a surface separation of the north wall from this ring. Between 56°W and 50°W there is a huge (123 km.) separation of the Harvard and Rutgers north walls. Figure 18b shows the enhanced AVHRR image of day 176 in this area, in which the north wall location is obvious, confirming the Rutgers analysis.

The reason for the large average offset of the Harvard north wall from the Rutgers analysis on June 29 (Table 5), is simply a discrepancy in recognizing the collapsing trough at 61°W (Figure 27). Figure 16 shows a Geosat track from day 182 running straight up this trough and a complete signal drop up the length of the trough. This may have been missed using the pass-minus-pass difference technique on the

Geosat data at Harvard. IR imagery from day 182 also confirmed the presence of this trough. Except for the meander crests on either side of the collapsing trough, the remainder of the north wall is extremely close throughout. Note that the Harvard north wall has suddenly jumped north 125 kilometers in 7 days and agrees with the Rutgers north wall in the area east of 54°W.

The final day, July 4, contains many differences between the analyses over the entire region (Figure 28). The overall Harvard offset from the Rutgers north wall is greatest at this time, with an average offset of 31.3 kilometers (Table 5). The Harvard and NOAA analyses are again two days after the Rutgers analysis, which could account for eastward offsets in meander regions. The Harvard analysis is offset to the southeast of the Rutgers analysis between 65°W and 59°W, but the NOAA analysis either agrees or is offset only slightly to the southeast. The Rutgers north wall location is supported by image enhancements in this area from July 4, and the trough at 57°W is supported by a Geosat track from day 188 (Figure 17). The final area of major discrepancy is at 52°W, where the Rutgers north wall has just absorbed a ring, creating a large meander. The Harvard and NOAA analyses negate this occurrence. With the absence of XBT and Geosat data during this time, and unclear surface imagery, this is one area that could be interpreted as either a ring or ring absorption, even though in the enhanced July 4 image there seems to be no thermal separation at the surface.

4.4 Summary and Future Improvements to Mapping Techniques

The NOAA, Harvard and warmest pixel composite derived north walls were compared to north walls derived using this study's improved mapping technique (Table 5). The maximum NOAA north wall offsets ranged from 55.4 to 225.0

kilometers. The average Harvard north wall offset ranged from 12.0 to 31.3 kilometers, whereas the maximum offsets ranged from 58.0 to 261.0 kilometers. The average warmest pixel north wall offsets ranged from 0.4 to 4.7 kilometers whereas the maximum offsets ranged from 7.7 to 40.0 kilometers. The average offsets calculated for the smaller regions of the warmest pixel composite ranged from 0.9 to 9.4 kilometers (Table 6), which is a more realistic result than the average offsets computed for the entire region.

. Improvements to the current analysis scheme could be made by incorporating additional data sets into the Geographic Information System environment. In situ velocity measurements obtained from ARGOS drifting buoys or moored current meters would be useful for comparisons to the current speeds estimated from the Geosat altimeter. Also, ARGOS buoys are especially useful for tracking rings and estimating their shape and swirl velocity (Glenn et al., 1990). Moored current meters would also identify rings or meanders that pass though their location due to changes in current velocity and direction.

Chapter 5

Comparisons of Geosat, AVHRR and XBT Derived Locations of the Gulf Stream North Wall

5.1 Introduction

The data set accumulated to create the surface maps of the Gulf Stream provides an excellent opportunity to compare the different data types to each other. Specifically, comparisons of Geosat maximum velocity axis to the AVHRR derived surface north wall and the XBT derived subsurface north wall are possible. The Gulf Stream maximum velocity axis is determined from the derivative of the along track dynamic topography as estimated from the Geosat altimeter using the Glenn et al. (1991a) synthetic geoid. The maximum velocity axis is where the slope of the sea surface height signal is at a maximum. The AVHRR derived surface north wall is created when an analyst subjectively estimates the north wall based on the warmest and largest sea surface temperature gradient. The XBT subsurface north wall is defined as the location of the 15^{o}C isotherm at a depth of 200 meters. Some of the XBT data are along-Geosat-track XBT drops. Linear interpolations of this 15^{o}C isotherm location were made between XBT's with temperature values straddling 15^{o}C. The Glenn and Robinson (1991) Gulf Stream temperature feature model indicates that linear interpolation is sufficiently accurate if the nominal 20 kilometer spacing between XBTs is maintained. The XBT's were dropped along Geosat tracks specifically for comparison testing.

5.2 Geosat Maximum Velocity Axis vs. the AVHRR Derived North Wall

Comparisons of the Gulf Stream maximum velocity axis locations derived from Geosat via the Glenn et al. (1991a) synthetic geoid were made to the Gulf Stream maximum temperature gradient north wall derived from nearly simultaneous (+/- 24 hours) sea surface temperature images. As forced by the availability of AVHRR data, the time period of these comparisons was from October 1987 to October 1988. There were 323 ascending and descending Geosat tracks during this time. There was clear (cloud free) imagery under these tracks within 24 hours only 67 times (20%). Lebanon et al. (1990) found that in creating similar north wall maps, 1/3 of all the north wall locations created were derived from Geosat data. These two facts indicate that Geosat is a very important component of Gulf Stream mapping. Table 7 lists these 67 comparable samples in chronological order, with lists of time offset, vector distance offset, angle at which the Geosat pass crossed the north wall in the IR imagery, and Geosat track number (Figure 3a). Vector offset is the distance and direction of the offset, with positive values indicating the IR north wall is north of the Geosat maximum velocity axis, and negative values indicating the IR north wall is south of the Geosat maximum velocity axis.

The entire data set was compared. For all 67 comparison days, the IR derived north wall was an average of 13.2 kilometers north of the Gulf Stream maximum velocity axis, with a root mean square (RMS) difference of 14.8 kilometers (Figure 29)(Table 8a). Cornillion and Watts (1987) compared the IR north wall location with the location of the 15^{o}C isotherm at 200 meters as derived from Inverted Echo Sounder (IES) data. They found the IR north wall to be an average of 9 kilometers north of the subsurface north wall with an RMS of 14.3 kilometers. Szczechowski (1991) compared IR imagery to the 15^{o}C isotherm at 200 meters as derived from

along-track XBT data, finding the surface north wall to be an average of 8 kilometers to the north of the subsurface front, with an RMS of 13.0 kilometers. The averages are different from each other because Cornillion and Watts (1987) and Szczechowski (1991) were comparing the IR to the subsurface north wall, not the Geosat maximum velocity axis. The RMS values are practically the same, however, and because most of the variability is usually assumed to be associated with the IR data, this implies that the variability of the Geosat derived maximum velocity axis locations are as stable as the IES or XBT data.

Several subsets of the data were constructed and compared. When sorting the comparisons by time differences between the satellite passes, and by the angle the Geosat altimeter crossed the Stream, there were no pronounced trends. The most interesting trend found was associated with meander shape. Both the average vector offset and the RMS variability in the vector offsets increase when moving from a meander trough (8.6 +/- 7.1 km.), to a straight Stream (11.6 +/- 9.9 km.), to a meander crest (20.2 +/- 21.8 km.) (Table 8a). The additional centripetal acceleration associated with the meander curvature in a meander trough forces surface water to the south, decreasing the Stream's width. The RMS variability is reduced due to the confining influence of the Gulf Stream itself (Figures 31 and 32). In meander crests, however, centripetal acceleration forces the surface water to the north, leading to an increase in RMS because the slope water does not act as a barrier, permitting the Stream to widen.

> "Where the Stream's flow is cyclonic (trough) the accelerations due to the Coriolis parameter and the curvature add leading to a narrower Stream with a steeper cross-stream slope of the sub-surface fronts. Conversely, where the Stream's flow is anticyclonic (crest) the accelerations due to the Coriolis parameter and the curvature are of opposite sign leading to wider Stream with a smaller cross-stream slope of the subsurface front. (Horton, 1986)"

This tightening of the Gulf Stream and increase in the slope of the subsurface front when moving from a meander crest to a trough was noted by Horton (1986) in the thermal record but was not confirmed in the velocity record until these comparisons to the Geosat maximum velocity axis were conducted.

When sorting the comparisons by longitudinal location (Geosat track number), there was a noted increase in RMS when moving downstream (eastward), but the average vector offset is the same in the west and central regions (Table 8a). The eastern region only contains 5 tracks thus results for this region may not be as reliable as those for the western and central regions. In the western region, the Stream is usually straight (Table 8b). The western region average vector offset and RMS values agree closely with the subset result comparisons of the straight Stream (Table 8a). Also, the most intense meandering occurs in the central region. In this central region one would expect an equal number of crests and troughs (Table 8b), but because the increase in RMS associated with crests is much greater than the decrease associated with troughs, there is an increase in these RMS values over those in the western or straight region.

5.3 Geosat Maximum Velocity Axis vs. XBT Subsurface North Wall

The second set of comparisons made were between the Gulf Stream maximum velocity axis locations and the 15^{o}C isotherm at a 200 meter depth as derived from along-Geosat-track XBT drops. The time period of these comparisons was between November 1986 and November 1988. There were a total of 41 comparisons possible within 24 hours. Some Geosat tracks were only partial tracks, however, and had to be eliminated; some XBT drops were bad. XBT's were dropped at 20 kilometer intervals along a Geosat track, but occasionally some of the XBTs fail. If the spacing of the XBT's straddling the 15^{o}C isotherm at 200 meters was 40 kilometers or greater (i.e.

one or more bad XBTs dropped consecutively), those data were considered invalid and were eliminated. The interpolation of the 15ºC isotherm location may not be accurate in these situations. Some comparisons were eliminated because the aircraft dropping the XBTs wandered off the Geosat track path, negating direct overlay of the paths. After eliminating the problem comparisons for the above reasons, a total of 28 comparisons remained. They are listed in Table 9, which contains similar columns to those in Table 7.

Again, comparisons were first made on the entire data set, resulting in an average northward displacement of the subsurface north wall from the maximum velocity axis of 8.9 kilometers, with an RMS of 11.2 kilometers (Table 10)(Figure 30). Szczechowski (1991) made similar comparisons of the XBT and Geosat data, but compared to the Geosat derived north walls instead of the axis. It was determined that the average northward displacement of the Geosat north wall from the subsurface north wall was 19 kilometers with an RMS of 14 kilometers. As previously discussed, the Geosat axis has a precise mathematical definition while the Geosat north wall is located subjectively by an analyst. Adding Szczechowski's average offset results to those attained in this study result in the Geosat surface north wall being located approximately 27.9 kilometers to the north of the Geosat maximum velocity axis, indicating that the velocity structure of the Gulf Stream is much wider than the thermal. However, Szczechowski's study was based on only 10 samples, making the results somewhat less reliable.

As with the AVHRR - Geosat comparisons, subset comparisons of the data were made. Again no trend with time was noted. The only significant results occurred when separating the data based on meander shape (Table 10). The average vector offset increases as one moves from meander trough, to a straight Stream, to a meander crest, agreeing with the expected effects of centripetal acceleration (Figures 31 and

32). As one moves from a trough to a crest, the Stream widens and the subsurface north wall slope decreases (Horton, 1986). The results here are strikingly similar to the vector offset comparisons of the Geosat maximum velocity axis to IR imagery in this study, except that the RMS of the Geosat/XBT meander crest vector offsets is very small. This could be due to the low number of samples (4).

5.4 XBT vs. AVHRR Derived North Walls

The final comparisons that were possible were of locations of the north wall derived from the AVHRR infrared imagery to the subsurface north wall as indicated by XBT surveys. The time period of these comparisons was from October 1987 to October 1988. Unfortunately, there were only 11 days where clear imagery was available below the XBT along-track drops. This is hardly enough to separate the comparisons by subsets (i.e. meander shape, time offset, track number). The average vector offset located the IR north wall 12.4 kilometers to the north of the XBT derived subsurface north wall, with an RMS of 7.5 kilometers (Table 11). Both Cornillion & Watts (1987) and Szczechowski (1991) made comparisons of the same data types, with similar results of 9.0 +/- 14 kilometers and 8.0 +/- 13.0 kilometers respectively. The slightly greater offset and lower RMS results of this study could be due to the small number of samples in the comparisons.

5.5 Summary

AVHRR sea surface temperature imagery and XBT thermal data within +/- 24 hours of a Geosat pass were compared to the Geosat velocity data using the Geosat interpreted maximum velocity axis as a datum. The AVHRR north wall was 13.2 +/-

14.8 kilometers north of the Geosat axis. The XBT derived subsurface north wall was 8.9 +/- 11.2 kilometers north of the Geosat axis. No trends were noted when the comparisons were sorted by time offset between the Geosat pass and the thermal data. For the AVHRR comparisons to the Geosat axis, a striking trend was noted with meander shape. In meander troughs, the average vector offset was 8.6 +/- 7.1 kilometers, in straight Gulf Stream areas the average vector offset was 11.6 +/- 9.9 kilometers, and in meander crests the average vector offset was 20.2 +/- 13.7 kilometers. This same trend of increasing vector offset with an increase in negative curvature was noticed in the XBT subsurface north wall comparisons to the Geosat maximum velocity axis. For the XBT/Geosat comparisons, the average vector offset for troughs was 5.4 +/- 5.2 kilometers, for a straight Stream 8.3 +/- 13.1 kilometers, and for a meander crest 17.7 +/- 3.2 kilometers. This result of a narrowing of the Stream with increased positive (cyclonic) curvature agrees with the expected effects of centripetal acceleration on the flow (Horton, 1986; Newton, 1978).

Chapter 6
Summary and Conclusions

The modern ocean forecast scheme consists of an observation network, statistical models and dynamical forecast models which are linked by one of several data assimilation schemes. Operational ocean forecasts using simplified dynamical models and basic assimilation schemes are currently being generated in the Gulf Stream region on a regular basis. With recent increases in computer speed and availability, forecast models are becoming more sophisticated and data assimilation schemes more complex. The increase in model sophistication and adoption of more elaborate data assimilation schemes will continue in the near future, necessitating more accurate initialization and verification data to test model improvements. This thesis is a major step towards improving the observation network component of the modern forecast scheme, producing the most accurate maps to date for testing the new generation of Gulf Stream forecast models. The incorporation of a GIS into the analysis scheme, the use of an accurate geoid, and the use of a new AVHRR compositing technique have all aided in creating these new, more accurate maps.

Compositing techniques for attaining mostly complete AVHRR infrared imagery over the Gulf Stream Ring and Meander Region are necessitated by cloud cover over the oceans. At present, the patching technique introduced in this thesis requires more human intervention than does the standard warmest pixel composite, but it does not smear ring and north wall shapes. Maintaining and mapping the true, unsmeared shapes of both the rings and the north wall is imperative when the maps are used to initialize and verify dynamic forecast models. These analyses also are more accurate when developed in the context of a Geographic Information System. All data that are input into this system maintain their exact geographic location. In previous

studies the registration of data on hard copy paper overlays maintained no exact geographic coordinates, contributing to spatial offsets in the final north wall and ring location estimates.

Of the three data types used to create the surface maps of the Gulf Stream, AVHRR infrared imagery was by far the most useful, providing more than 60% of the data. Geosat and XBT data only provided small segments of the north wall or occasionally located rings not visible in the imagery. This conclusion on data importance, however, is specific to this data rich time period. The days chosen in this study were selected based on the clarity of the AVHRR imagery, because the imagery can provide almost complete coverage across the region during cloud free periods. In times of spatially extensive cloud cover over long periods of time (e.g., winter), AVHRR is useless, whereas Geosat and XBT data are still usable. Previous studies found that in creating similar north wall and ring maps over an entire year, Geosat provided about 1/3 of the information (30%). Because previous studies found that Geosat data contributed to 30% of all mapped data and this study found that 80% of all Geosat tracks occurred in cloudy areas of the imagery, the importance of the Geosat satellite altimeter to Gulf Stream mapping and the importance of the Geosat Follow On Mission scheduled to begin in 1995 are highlighted.

The comparisons of the Geosat maximum velocity axis to the AVHRR-derived north wall and to the XBT-derived subsurface north wall indicate the Gulf Stream acts like the Jet Stream when meandering. The Gulf Stream widens and the subsurface north wall slope flattens in meander crests, whereas in meander troughs, the subsurface north wall slope is steep and the Stream is thinner. Also, the RMS values attained from comparing AVHRR and XBT locations to the Geosat maximum velocity axis are similar to those from previous studies, indicating the Geosat altimeter signal is a stable means of estimating the location of the Gulf Stream's axis.

The present study demonstrates the differences in the Gulf Stream structure for troughs, crests, and flat Stream regions. Now it is necessary to reexamine these results more carefully. Radius of curvature estimates of the north wall can be made from the imagery. A continuous graph of the offsets and RMS versus Gulf Stream curvature could be constructed, as opposed to just the three category separation of meander crest, meander trough, and flat Stream used here.

In previous mapping projects, including this one, ARGOS buoy data and current meter data were not used. ARGOS buoys are free floating buoys that are occasionally dropped by both government and private sources into areas of scientific interest, including the Gulf Stream Ring and Meander region. The NOAA polar orbiting platforms collect the locations of these buoys every several hours. Over a period of a few months, these buoys provide an archive of the paths of the currents they followed. A plot of this path can help locate rings, Gulf Stream meanders, and estimate current speeds. Including this ARGOS buoy data would improve the accuracy of the north wall analyses, and would improve estimates of ring rotational speeds that are currently estimated from the Geosat altimeter data. Current meter data from multiple sources, now being made available from 1988, would make comparison testing to estimated current speeds from the Geosat altimeter and ARGOS buoys possible.

The topic of oceanography has generally been ignored in GIS research. GIS software packages are built with land analyses in mind, not oceanographic analyses. In future projects at Rutgers, the GRASS software package will not be used. A new public domain software package recently developed by the Naval Research Lab called Naval Satellite Image Processing System (NSIPS) will be used. It includes most of the image analysis functions that GRASS does, but it also includes software to analyze and display multiple raw XBT data types and multiple raw altimeter data formats,

including Geosat, TOPEX, ERS-1 and the soon to be launched Geosat Follow On satellite.

In a few years there will be multiple satellite altimeters such as the Geosat Follow On satellite, TOPEX, and ERS-1. These will all be used for mapping currents because they all penetrate cloud cover, which complements AVHRR imagery, and they have different orbital tracks over the earth's surface, which negates repetition of data. These three different altimeters will require different geoids and different algorithms for correcting and georeferencing the raw data. Also, with the large increases in daily data production expected with the launching of new satellites in the near future (i.e., Earth Observing Satellite - EOS, Geosat Follow On), it will be important to have a software package that limits the amount of time necessary to import and analyze the multiple data formats. The less time an analyst spends importing data, the more time the analyst has to analyze the data.

The future of Gulf Stream mapping is expert system analysis, which could not only automatically import AVHRR, Geosat, XBT, and Argos buoy data, but make maps of the north wall and ring locations either without or with very little human intervention. Computer speeds are continuously increasing, and costs are decreasing, making expert system research possible to both government and private firms. Currently, a Naval Research Laboratory group at the Stennis Space Center, Mississippi, is working on an expert system that interpolates wall and ring locations from AVHRR imagery. In their system the computer searches for the large thermal gradients in the imagery and creates lines in those areas. Labels (north wall, cold ring, warm ring) are then given to these lines based on latitudinal location. The computer then fits a north wall to the intermittent lines, and fits circular rings to those lines labeled as rings. However, this system is in its early stages and is not very accurate. One improvement would be to use an automated patching technique instead of

warmest pixel composites. After removing the clouds from the latest image using a predefined cloud detection algorithm, the image could be patched over an existing composite, thereby updating the older composite with the new data. The composite could be updated continuously as new data arrive. The result would be a composite image like those created in this study, which improved the human analysis accuracy. Even with these automated computer analyses, it will still be difficult to take the human element completely out of the analysis loop. It is apparent that the "man-machine mix" which was so important in the early days of meteorological weather forecasting is still important today during the infancy of ocean forecasting.

Table 1: The type and date (Julian Calendar day) of data used for analysis in each mapped day (Figures 11-17). Note that the order of days for images indicates the order in which the images were "patched" on top of one another in layer cake fashion. Note also that unless otherwise noted, all Geosat tracks are ascending. XBTs are listed by source (Institute for Naval Oceanography - INO, Harvard University - HARV, University of Rhode Island - URI, NAVOCEANO - NAV), then day.

Modeled Day	AVHRR Images	Geosat Tracks	AXBTs
May 25th	146, 145, 147	143, 144 (descend), 145, 146, 148, 149	INO - 147
May 30th	151, 153, 148	148, 149, 150, 151, 152, 153, 154	HARV - 153 INO - 150, 151, 152, 153
June 5th	157, 158, 155, 159, 160, 154	154, 156, 157, 158, 159, 160	INO - 155, 156, 157
June 13th	165, 166, 163, 167,168	161, 164, 165, 166	INO - 162, 163, 164 NAV - 164 a-b, 167 a-b
June 22nd	174, 176, 173, 175	171, 173, 174, 176, 177	INO - 172, 174, 175 NAV - 171 a-b, 174 a-b URI - 174
June 29th	180, 181, 182, 178	178, 178 (descend), 179, 180, 180 (descend), 181, 182, 183, 184	INO - 181, 182, 183 URI - 182
July 4th	186, 185,187, 184	184, 185, 187, 188	INO - 183, 189

Table 2: Satellite and in situ data used to locate warm and cold rings for each study date.

Date/ Ring	W1	W2	W3	W4	W5
May 25	AVHRR	AVHRR XBT	**not yet formed	AVHRR Geosat	Geosat
May 30	AVHRR Geosat	AVHRR	AVHRR Geosat XBT	Interpolated	AVHRR Geosat
June 5	AVHRR	AVHRR Geosat	AVHRR	AVHRR Geosat	Interpolated
June 13	AVHRR XBT	AVHRR	AVHRR Geosat XBT	AVHRR	Geosat XBT
June 22	AVHRR	AVHRR Geosat XBT	AVHRR	AVHRR Geosat XBT	AVHRR XBT
June 29	AVHRR	AVHRR	AVHRR	AVHRR	AVHRR
July 4	AVHRR	AVHRR Geosat	AVHRR	AVHRR	**Absorbed by meander

Date/ Ring	C1	C2	C3	C4	C5
May 25	AVHRR	AVHRR	AVHRR Geosat XBT	Interpolated	Geosat
May 30	AVHRR	Interpolated	AVHRR Geosat XBT	AVHRR Geosat XBT	Interpolated
June 5	AVHRR	AVHRR Geosat	AVHRR	Geosat	Interpolated
June 13	AVHRR	AVHRR	AVHRR Geosat	Interpolated	Interpolated
June 22	Interpolated	Interpolated	**Absorbed by meander	AVHRR Geosat	AVHRR Geosat
June 29	AVHRR	Interpolated	**Absorbed by meander	Interpolated	Geosat
July 4	AVHRR	AVHRR	AVHRR	AVHRR Geosat	Interpolated

Table 3: Average speeds (km/day) and compass directions of ring centers between study days. Values in *italics* indicate periods that contain interpolated ring centers.

AAS
Comment [2]: Page: 1

Ring/ Dates	May 25-May 30	May 30-June 5	June 5-June 13	June 13-June 22	June 22-June 29	June 29-July4
W1	7.25 w	2.66 w	3.97 sw	3.06 sw	7.71 wsw	7.11 wsw
W2	10.14 nw	1.18 s	5.25 wsw	5.70 sw	4.60 ssw	5.16 nw
W3	**not yet formed	2.13 e	1.19 w	7.16 nne	14.08 ne	15.54 nw
W4	*9.51 wnw*	*2.76 ne*	6.78 w	3.46 ne	15.37 se	2.05 sse
W5	1.64 se	*5.39 e*	*4.56 e*	4.58 e	8.28 ssw	Absorbed by meander

Ring/ Dates	May 25-May 30	May 30-June 5	June 5-June 13	June 13-June 22	June 22-June 29	June 29-July 4
C1	3.68 ene	0.86 se	1.64 sw	*1.06 sw*	*1.07 sw*	1.09 sw
C2	*4.88 wnw*	*4.83 wnw*	4.88 wnw	*2.60 wsw*	*2.57 wsw*	*2.61 wsw*
C3	6.06 e	6.09 sw	10.09 se	absorbed by meander	absorbed by meander	new ring created
C4	*1.27 s*	1.20 s	*0.32 sw*	*0.56 s*	*7.52 w*	*7.53 w*
C5	*2.74 wsw*	*4.37 wsw*	*4.33 wsw*	*4.33 wsw*	9.55 wsw	*10.26 wsw*

Table 4: Ring locations (latitude, longitude), radius(e), radius(max), radius(o) and estimated rotation speed based on the Geosat Altimeter. Rad(max)=0.75*rad(e). Rad(o)= (rad(max)/0.6). Note that calculated radius(e) is an average of the semi-major and semi-minor axis of elliptical rings.

May 25:

Ring	Latitude	Longitude	Radius(e) km	Rad(max) km	Rad(o) km	Speed cm/sec
W1	39.2384 N	69.0250 W	70.3	52.7	87.8	100
W2	39.6881 N	65.5000 W	84.4	63.3	105.5	125
W4	41.2551 N	57.6750 W	86.1	64.6	107.6	100
W5	41.4235 N	54.0750 W	100.0	75.0	125.0	100
C1	34.1011 N	73.1500 W	64.1	48.1	80.1	125
C2	34.7090 N	69.5743 W	58.0	43.5	72.5	100
C3	37.3195 N	60.7581 W	47.8	35.9	59.8	200
C4	37.2351 N	56.9087 W	48.0	36.0	60.0	75
C5	37.7425 N	52.3605 W	65.0	48.8	81.3	100

May 30:

Ring	Latitude	Longitude	Radius(e) km	Rad(max) km	Rad(o) km	Speed cm/sec
W1	39.2770 N	69.4250 W	75.9	57.0	94.9	100
W2	40.0065 N	65.8750 W	82.1	61.6	102.7	125
W3	40.3684 N	62.8250 W	97.9	73.4	122.3	200
W4	41.3113 N	58.2000 W	61.4	46.4	77.3	100
W5	41.3674 N	54.0250 W	100.0	75.0	125.0	100
C1	34.1424 N	72.9500 W	63.0	47.3	78.8	125
C2	34.7443 N	69.8408 W	57.9	43.4	72.4	100
C3	37.3600 N	60.4250 W	57.9	43.5	72.4	200
C4	37.1814 N	56.9250 W	47.3	35.4	59.1	75
C5	37.6964 N	52.5064 W	65.0	48.8	81.3	100

June 5:

Ring	Latitude	Longitude	Radius(e) km	Rad(max) km	Rad(o) km	Speed cm/sec
W1	39.2963 N	69.6000 W	82.1	61.6	102.7	100
W2	39.9492 N	65.8999 W	97.9	73.4	122.3	125
W3	40.4063 N	62.7000 W	91.7	68.8	114.6	200
W4	41.3861 N	58.0499 W	75.9	57.0	94.9	100
W5	41.3674 N	53.6673 W	94.5	70.9	118.1	100
C1	34.1217 N	72.8999 W	68.6	51.5	85.8	125
C2	34.7886 N	70.1606 W	57.7	43.3	72.1	100
C3	37.1417 N	60.7250 W	48.4	36.3	60.5	200
C4	37.1169 N	56.9446 W	46.4	34.7	58.0	75
C5	37.6641 N	52.7945 W	65.0	48.8	81.3	100

June 13:

Ring	Latiutude	Longitude	Radius(e) km	Rad(max) km	Rad(o) km	Speed cm/sec
W1	39.0838 N	69.8250 W	87.8	65.8	109.7	100
W2	39.8536 N	66.3500 W	101.8	76.4	127.3	125
W3	40.3691 N	62.7942 W	104.1	78.0	130.1	200
W4	41.4235 N	58.6499 W	75.4	56.6	94.3	100
W5	41.3674 N	53.2590 W	87.1	65.3	108.9	100

C1	34.0598 N	73.0250 W	55.1	41.3	68.9	125
C2	34.8700 N	70.5815 W	57.5	43.1	71.9	100
C3	36.6430 N	60.0750 W	73.1	54.8	91.4	200
C4	37.1088 N	56.9707 W	45.2	33.9	56.5	75
C5	37.6210 N	53.1786 W	65.0	48.8	81.3	100

June 22:

Ring	Latitude	Longitude	Radius(e) km	Rad(max) km	Rad(o) km	Speed cm/sec
W1	38.9331 N	70.0634 W	92.8	69.6	116.0	100
W2	39.6043 N	66.8250 W	105.2	78.9	131.5	125
W3	40.8981 N	62.6250 W	75.4	56.5	94.2	125
W4	41.5542 N	58.3500 W	86.1	64.5	107.6	100
W5	41.3674 N	52.7999 W	78.8	59.1	98.4	100
C1	34.0016 N	73.1094 W	51.3	38.5	64.2	125
C2	34.8010 N	70.8288 W	59.6	44.7	74.5	100
C4	37.0621 N	57.0000 W	43.9	32.9	54.8	75
C5	37.5726 N	53.6102 W	65.0	48.8	81.3	100

June 29:

Ring	Latitude	Longitude	Radius(e) km	Rad(max) km	Rad(o) km	Speed cm/sec
W1	38.8317 N	70.6500 W	65.8	49.4	82.3	100
W2	39.3734 N	67.0250 W	93.9	70.5	117.4	125
W3	41.3861 N	61.7500 W	55.1	41.3	68.9	125
W4	41.1238 N	57.2999 W	77.1	57.8	96.3	100
W5	40.9734 N	52.4250 W	75.4	56.5	94.2	100
C1	33.9564 N	73.1750 W	48.4	36.3	60.5	125
C2	34.7473 N	71.0211 W	61.2	45.9	76.5	100
C4	37.0737 N	57.5833 W	43.3	32.4	54.0	75
C4	37.4679 N	54.3361 W	65.0	48.8	81.3	100

July 4:

Ring	Latitude	Longitude	Radius(e) km	Rad(max) km	Rad(o) km	Speed cm/sec
W1	38.7345 N	71.0250 W	83.8	62.9	104.8	100
W2	39.5467 N	67.2000 W	100.0	75.0	125.0	125
W3	41.6831 N	62.5122 W	72.6	54.5	90.8	125
W4	41.0486 N	57.2500 W	74.3	55.7	92.8	100
C1	33.9240 N	73.2219 W	46.3	34.7	57.9	125
C2	34.7090 N	71.1585 W	62.4	46.8	78.0	100
C3	37.8342 N	60.4979 W	74.8	56.1	93.5	200
C4	37.0422 N	58.0000 W	42.8	32.1	53.4	75
C5	37.3852 N	54.9006 W	65.0	48.8	81.3	100

Table 5: Average and maximum offsets (in kilometers) of north wall locations from those north walls generated at Rutgers. Note that the calendar days of the Harvard and NOAA maps are not all the same as those done at Rutgers.

Rutgers Date (Julian Day)	Harvard and NOAA Julian Day	NOAA Maximum Offset	Harvard Offset		Warmest Pixel Offset	
			Avg.	Max.	Avg.	Max.
May 25 (146)	146	78.8	15.5	58.0	4.7	28.3

May 30 (151)	153	199.4	15.7	75.8	2.7	27.1
June 5 (157)	160	117.5	29.2	145.3	2.2	26.0
June 13 (165)	167	55.4	12.0	147.4	4.5	28.1
June 22 (174)	174	191.3	21.3	123.5	2.3	24.0
June 29 (181)	181	91.6	22.4	261.0	0.4	7.7
July 4 (186)	188	225.0	31.3	181.1	3.9	40.0

Table 6: Average offsets of warmest pixel derived north walls from north walls derived using this study's technique in the defined regions. These regions are areas where patched north wall derivations were not inserted into cloudy areas of the warmest pixel composite. The average offsets of the entire Gulf Stream Ring and Meander region are also shown.

Day	**Region**	**Offset in Subset Region**	**Offset for Entire Region**
May 25	72°W - 57°W	5.3 km.	4.7 km.
May 30	74°W - 62°W	5.7 km.	2.7 km.
June 5	74°W - 62°W	3.4 km.	2.2 km.
June 13	74°W - 65°W	9.3 km.	4.5 km.
June 22	74°W - 66°W	6.6 km.	2.3 km.
June 29	74°W - 63°W	0.9 km.	0.4 km.
July 4	74°W - 63°W	9.4 km.	3.9 km.

Table 7: Comparisons of Geosat maximum velocity axis with AVHRR north wall. The following are column definitions:

Year / Day : Year and Julian calendar day of AVHRR image.
Time Offset : Time offset with (+) indicating Geosat pass after AVHRR pass.
Offset (km) : Vector distance between Geosat maximum velocity axis and AVHRR north wall. Positive (negative) values indicate the AVHRR north wall is north (south) of the Geosat maximum velocity axis.
Placement : +1: meander crest; 0 : flat stream; -1: meander trough.
Angle : Measured from the north wall (clockwise) to the Geosat zero crossing. For angles < 180 the IR north wall is north of the Geosat maximum velocity axis, wheras angles > 180 indicate the IR north wall is south of the Geosat maximum velocity axis.
Track # : Geosat track as indicated in Figure 3a.

Year / Day	Time Offset	Offset (km)	Placement	Angle	Track #
1987 / 294	-04.33	49.74	+1	110	A5
/ 296	+15.56	00.00	+1	80	A6
/ 300	-03.15	03.25	-1	5	A7
/ 303	-18.12	00.00	+1	80	D3
/ 308	-14.11	04.46	-1	100	A4
/ 308	-00.06	11.19	-1	75	D5
/ 308	-00.06	18.80	-1	75	D5
/ 308	-00.06	45.76	+1	90	D5
/ 308	+09.30	06.35	+1	30	A10
/ 312	-18.02	-15.11	0	240	A11
/ 313	+20.52	15.53	+1	80	A6
/ 313	-18.09	01.26	+1	45	A17
/ 314	+10.45	21.50	0	45	A12
/ 319	-01.22	08.60	0	100	A2
/ 319	+22.08	12.66	-1	105	A8
/319	+22.08	-15.93	-1	225	A8
/ 319	+22.08	27.30	+1	90	A8
/ 320	-06.16	34.29	+1	105	A8
/ 320	-17.34	41.94	+1	95	A8
/ 353	-14.24	-05.97	0	280	A2
88 / 017	-22.45	17.04	+1	90	A17
/ 017	+02.23	15.44	0	100	A6
/ 019	+22.19	11.82	+1	70	A7
/ 040	-10.44	78.00	+1	100	A8
/ 048	-10.19	15.34	0	65	A5
/ 053	+17.18	10.33	-1	30	A7
/ 061	+04.12	16.19	-1	110	D10
/ 062	+05.31	08.03	0	80	A4
/ 062	-05.53	-02.10	0	240	A4
/ 062	+08.00	03.86	-1	130	D5
/ 068	+05.10	07.53	-1	90	A6
/ 069	-18.39	05.86	-1	105	A6
/ 080	-14.53	22.19	+1	90	D5
/ 083	-21.13	15.61	0	70	A5
/ 083	-07.20	11.02	-1	70	D6

Table 7: Continued.

/ 083	-14.14	13.57	-1	70	D6
/ 090	-03.40	24.36	0	90	A2
/ 090	+10.14	18.79	0	135	D3
/ 091	-20.48	27.20	0	100	A2
/ 091	-13.36	16.90	0	115	D3
/ 093	+20.29	04.02	+1	40	A9
/ 111	-18.53	03.52	0	70	A3
/ 114	-19.19	06.38	0	75	A4
/ 114	-05.27	03.58	+1	75	D5
/ 117	-14.49	02.98	0	65	A5
/ 120	-18.36	07.12	-1	90	A6
/ 125	-00.17	06.52	-1	145	D3
/ 126	-14.30	-10.77	+1	240	A8
/ 134	-13.52	12.02	-1	35	A5
/ 134	00.00	07.67	0	110	D6
/ 141	+10.36	16.18	0	90	A2
/ 145	+10.55	07.77	0	65	A9
/ 151	-12.56	04.64	+1	35	A5
/ 153	+00.05	16.61	-1	75	A6
/ 157	-23.03	14.80	-1	110	A7
/ 160	-12.39	08.20	+1	80	A8
/ 164	+01.24	11.63	0	90	A4
/ 165	+12.32	12.57	-1	120	A10
/ 165	-10.58	11.51	0	90	A4
/ 170	+12.28	19.51	0	95	A6
/ 171	-22.47	03.81	0	65	A6
/ 187	+13.25	14.76	0	70	A6
/ 211	+15.22	43.97	+1	115	A14
/ 240	-17.40	17.20	0	85	A12
/ 256	-02.24	04.05	-1	100	D7
/ 257	-14.50	04.49	-1	100	D7
/ 266	+18.31	28.76	0	45	A4

Table 8a: Average offsets, RMS values, and total samples of data subsets of the comparisons of the Geosat maximum velocity axis to the AVHRR north wall.

Offset (km)	RMS	Samples (N)	Data Subset
13.2	14.8	67	All data
8.6	7.1	21	Meander troughs
11.6	9.9	26	Straight stream
20.2	21.8	20	Meander crest
13.0	10.5	42	West (tracks 01A-06A, 02D-06D)
17.0	17.1	20	Central (tracks 07A-011A, 07D-10D)
20.2	13.7	5	East (tracks 12A-17A, 11D-16D)

Table 8b:

Meander Placement	Western Region	Central Region	Eastern Region	Totals
Crest	8	9	3	20
Straight Stream	22	2	2	26
Trough	12	9	0	21
Totals	42	20	5	67

Table 9: Comparison of Geosat maximum velocity axis to the XBT 15°C isotherm at 200 meter depth. The following are column definitions:

Year / Day : Year and Julian calendar day of the Geosat pass.
Time Offset : Time offset (decimal day) with (+) indicating Geosat pass after XBT drop.
Offset (km) : Vector distance between the Geosat maximum velocity axis and the XBT 15°C isotherm at a 200 meter depth. Positive (negative) values indicate the XBT subsurface north wall is north (south) of the Geosat maximum velocity axis.
Placement : +1: meander crest; 0: straight Stream; -1: meander trough.
Track # : Geosat track as indicated by Figure 3a.

Year / Day	Time Offset	Vector Offset (km)	Placement	Track #
1986 / 341	+0.34478	4.2	0	A7
/ 344	-0.61352	27.2	0	A8
/ 346	-0.34454	12.4	0	A3
/ 349	-0.37122	-19.4	0	A4
1987 / 100	-0.00172	10.0	0	A3
/ 101	+0.76472	-23.6	0	A9
/ 112	-0.21913	12.9	0	A7
/ 126	-0.24142	11.6	-1	A6
/ 127	+0.87807	15.2	+1	A12
/ 129	-0.04813	10.6	0	A7
/ 130	-0.06664	8.3	-1	A13
/ 131	+0.78478	24.4	0	A2
/ 144	-0.20371	5.7	-1	A12
/ 146	-0.05598	13.8	0	A7
/ 147	+0.00809	2.7	-1	A13
/ 148	+0.84950	18.7	0	A2
1988 / 011	-0.26089	4.8	0	A4
/ 012	-0.34031	-5.4	-1	A10
/ 017	-0.20776	9.7	0	A6
/ 018	+0.57904	9.7	-1	A12
/ 020	-0.18136	7.4	0	A7
/ 022	-0.43158	18.6	0	A2
/ 164	+0.12926	13.6	0	A4
/ 167	+0.03936	21.4	+1	A5
/ 171	+0.22547	13.9	+1	A12
/ 173	+0.12227	5.1	-1	A7
/ 313	-0.41447	20.1	+1	A8
/ 318	-0.54263	-4.3	0	A4

Table 10: Average offsets, RMS values, and total samples of data subsets from the comparisons of the Geosat maximum velocity axis to the XBT 15^{O}C isotherm at a 200 meter depth.

Average Offset	RMS	Samples (N)	Data Subset
8.9	11.2	28	All Data
5.4	5.2	7	Meander troughs
8.3	13.1	17	Straight stream
17.7	3.2	4	Meander crest

Table 11: Comparisons of AVHRR derived north wall to the 15^{O}C isotherm at 200 meters as derived from XBT along track surveys. The day is the day of the AVHRR image, while a positive offset indicates the IR front is north of the XBT derived north wall. All comparisons are within +/- 24 hours.

Julian Day	Offset (Kilometers)
1988 / 153	16.61
157	14.80
160	8.20
1164	11.63
165	12.57
165	11.51
170	19.51
171	03.81
256	04.05
257	04.49
266	28.76
	AVG. = 12.36
	RMS. = 7.53

Appendix A: Comparisons of Geosat maximum velocity axis with AVHRR north wall. The following are column definitions:

Year / Day : Year and Julian calendar day of AVHRR image.

Time Offset : Time offset with (+) indicating Geosat pass after AVHRR pass.
Offset (km) : Distance between maximum velocit axis and AVHRR north wall.
Placement : +1: meander crest, 0 : flat stream, -1: meander trough.
Angle : Measured from the north wall (clockwise) to the Geosat zero crossing. For angles < 180 the Geosat maximum velocity is south of the north wall, while angles > 180 indicate the maximum velocity is north of the north wall.
Track # : Geosat track as indicated in figure 2.

Year / Day	Time Offset	Offset (km)	Placement	Angle	Track #
1987 / 294	-04.33	49.74	+1	110	A5
/ 296	+15.56	00.00	+1	80	A6
/ 300	-03.15	03.25	-1	5	A7
/ 303	-18.12	00.00	+1	80	D3
/ 308	-14.11	04.46	-1	100	A4
/ 308	-00.06	11.19	-1	75	D5
/ 308	-00.06	18.80	-1	75	D5
/ 308	-00.06	45.76	+1	90	D5
/ 308	+09.30	06.35	+1	30	A10
/ 312	-18.02	15.11	0	240	A11
/ 313	+20.52	15.53	+1	80	A6
/ 313	-18.09	01.26	+1	45	A17
/ 314	+10.45	21.50	0	45	A12
/ 319	-01.22	08.60	0	100	A2
/ 319	+22.08	12.66	-1	105	A8
/319	+22.08	15.93	-1	225	A8
/ 319	+22.08	27.30	+1	90	A8
/ 320	-06.16	34.29	+1	105	A8
/ 320	-17.34	41.94	+1	95	A8
/ 353	-14.24	05.97	0	280	A2
88 / 017	-22.45	17.04	+1	90	A17
/ 017	+02.23	15.44	0	100	A6
/ 019	+22.19	11.82	+1	70	A7
/ 040	-10.44	78.00	+1	100	A8
/ 048	-10.19	15.34	0	65	A5
/ 053	+17.18	10.33	-1	30	A7
/ 061	+04.12	16.19	-1	110	D10
/ 062	+05.31	08.03	0	80	A4
/ 062	-05.53	02.10	0	240	A4
/ 062	+08.00	03.86	-1	130	D5
/ 068	+05.10	07.53	-1	90	A6
/ 069	-18.39	05.86	-1	105	A6
/ 080	-14.53	22.19	+1	90	D5
/ 083	-21.13	15.61	0	70	A5
/ 083	-07.20	11.02	-1	70	D6
/ 083	-14.14	13.57	-1	70	D6
/ 090	-03.40	24.36	0	90	A2
/ 090	+10.14	18.79	0	135	D3
/ 091	-20.48	27.20	0	100	A2
/ 091	-13.36	16.90	0	115	D3

/ 093	+20.29	04.02	+1	40	A9
/ 111	-18.53	03.52	0	70	A3
/ 114	-19.19	06.38	0	75	A4
/ 114	-05.27	03.58	+1	75	D5
/ 117	-14.49	02.98	0	65	A5
/ 120	-18.36	07.12	-1	90	A6
/ 125	-00.17	06.52	-1	145	D3
/ 126	-14.30	10.77	+1	240	A8
/ 134	-13.52	12.02	-1	35	A5
/ 134	00.00	07.67	0	110	D6
/ 141	+10.36	16.18	0	90	A2
/ 145	+10.55	07.77	0	65	A9
/ 151	-12.56	04.64	+1	35	A5
/ 153	+00.05	16.61	-1	75	A6
/ 157	-23.03	14.80	-1	110	A7
/ 160	-12.39	08.20	+1	80	A8
/ 164	+01.24	11.63	0	90	A4
/ 165	+12.32	12.57	-1	120	A10
/ 165	-10.58	11.51	0	90	A4
/ 170	+12.28	19.51	0	95	A6
/ 171	-22.47	03.81	0	65	A6
/ 187	+13.25	14.76	0	70	A6
/ 211	+15.22	43.97	+1	115	A14
/ 240	-17.40	17.20	0	85	A12
/ 256	-02.24	04.05	-1	100	D7
/ 257	-14.50	04.49	-1	100	D7
/ 266	+18.31	28.76	0	45	A4

Appendix B: Comparison of Geosat maximum veloctiy axis to the XBT 15^{o}C isotherm at 200 meter depth. The following are column definitions:

Year / Day : Year and Julian calendar day of the Geosat pass.

Time Offset : Time offset (decimal day) with (-) indicating XBT drop before the Geosat pass.

Offset (km) : Distance between Geosat axis and the XBT 15^{o}C isotherm at a 200 meter depth. (-) indicates the Geosat axis is north of the XBT derived north wall.
Placement : +1: meander crest, 0: straight stream, -1: meander trough.
Track # : Geosat track as indicated by figure 2.

Year / Day	Time Offset	Offset (km)	Placement	Track #
1986 / 341	- 0.34478	4.2	0	A7
/ 344	0.61352	27.2	0	A8
/ 346	0.34454	12.4	0	A3
/ 349	0.37122	-19.4	0	A4
1987 / 100	0.00172	10.0	0	A3
/ 101	-0.76472	-23.6	0	A9
/ 112	0.21913	12.9	0	A7
/ 126	0.24142	11.6	-1	A6
/ 127	-0.87807	15.2	+1	A12
/ 129	0.04813	10.6	0	A7
/ 130	0.06664	8.3	-1	A13
/ 131	-0.78478	24.4	0	A2
/ 144	0.20371	5.7	-1	A12
/ 146	0.05598	13.8	0	A7
/ 147	-0.00809	2.7	-1	A13
/ 148	-0.84950	18.7	0	A2
1988 / 011	0.26089	4.8	0	A4
/ 012	0.34031	-5.4	-1	A10
/ 017	0.20776	9.7	0	A6
/ 018	-0.57904	9.7	-1	A12
/ 020	0.18136	7.4	0	A7
/ 022	0.43158	18.6	0	A2
/ 164	-0.12926	13.6	0	A4
/ 167	-0.03936	21.4	+1	A5
/ 171	-0.22547	13.9	+1	A12
/ 173	-0.12227	5.1	-1	A7
/ 313	0.41447	20.1	+1	A8
/ 318	0.54263	-4.3	0	A4

Figures

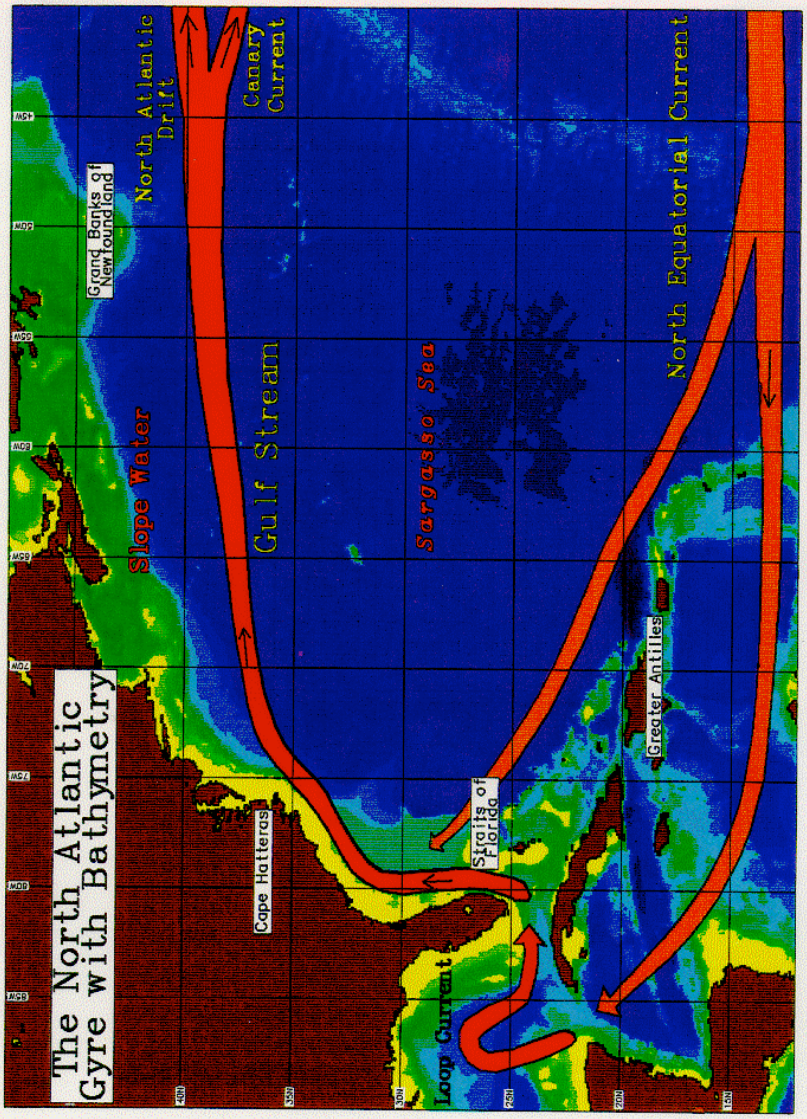

Figure 1: The North Atlantic Gyre. Bathymetry is displayed with yellow areas representing shallow water (less than 100 meters) and dark blue areas representing deep water (greater than 3500 meters).

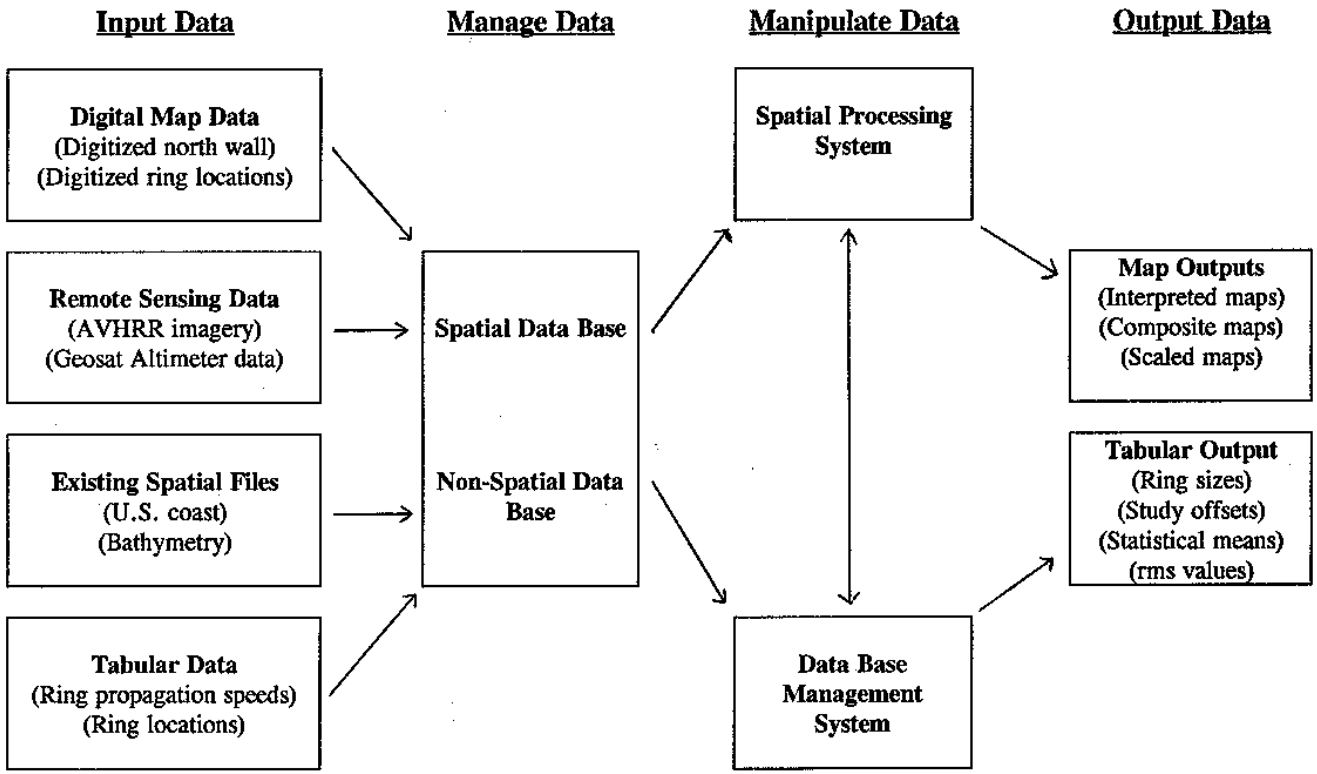

Figure 2: Flow chart of data movement through a Geographic Information system. Examples from this project are given in parentheses.

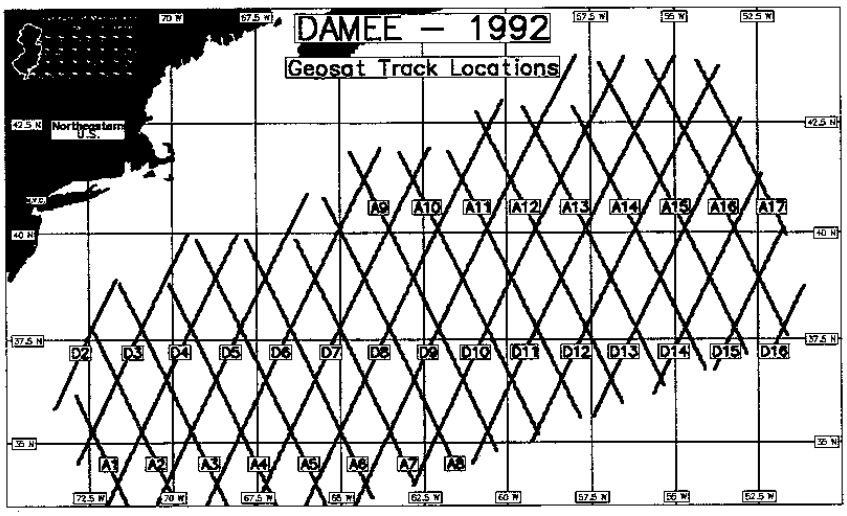

Figure 3a: All ascending and descending Geosat paths in the Gulf Stream Meander and Ring Region.

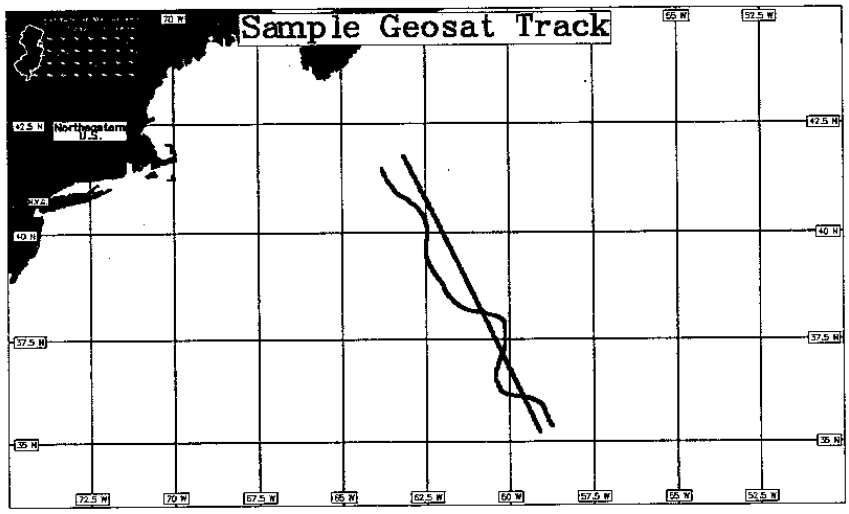

Figure 3b: A typical ascending Geosat track. The ground track and geoid are indicated by the straight line, whereas the curved line represents the relative height offset from the geoid. Heights above the geoid are to the right of the line, whereas negative heights are to the left (+/- 0.6 meter maximum).

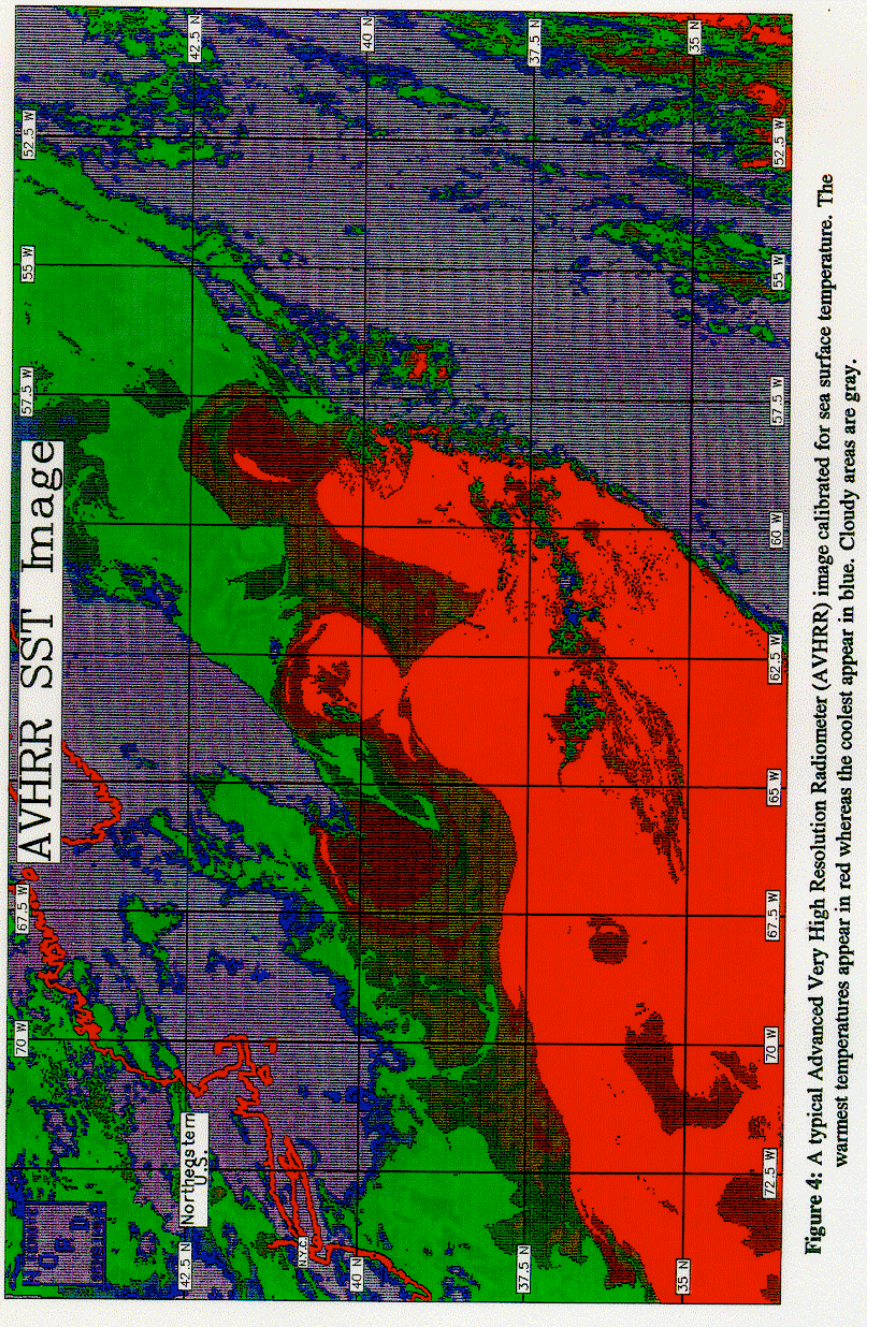

Figure 4: A typical Advanced Very High Resolution Radiometer (AVHRR) image calibrated for sea surface temperature. The warmest temperatures appear in red whereas the coolest appear in blue. Cloudy areas are gray.

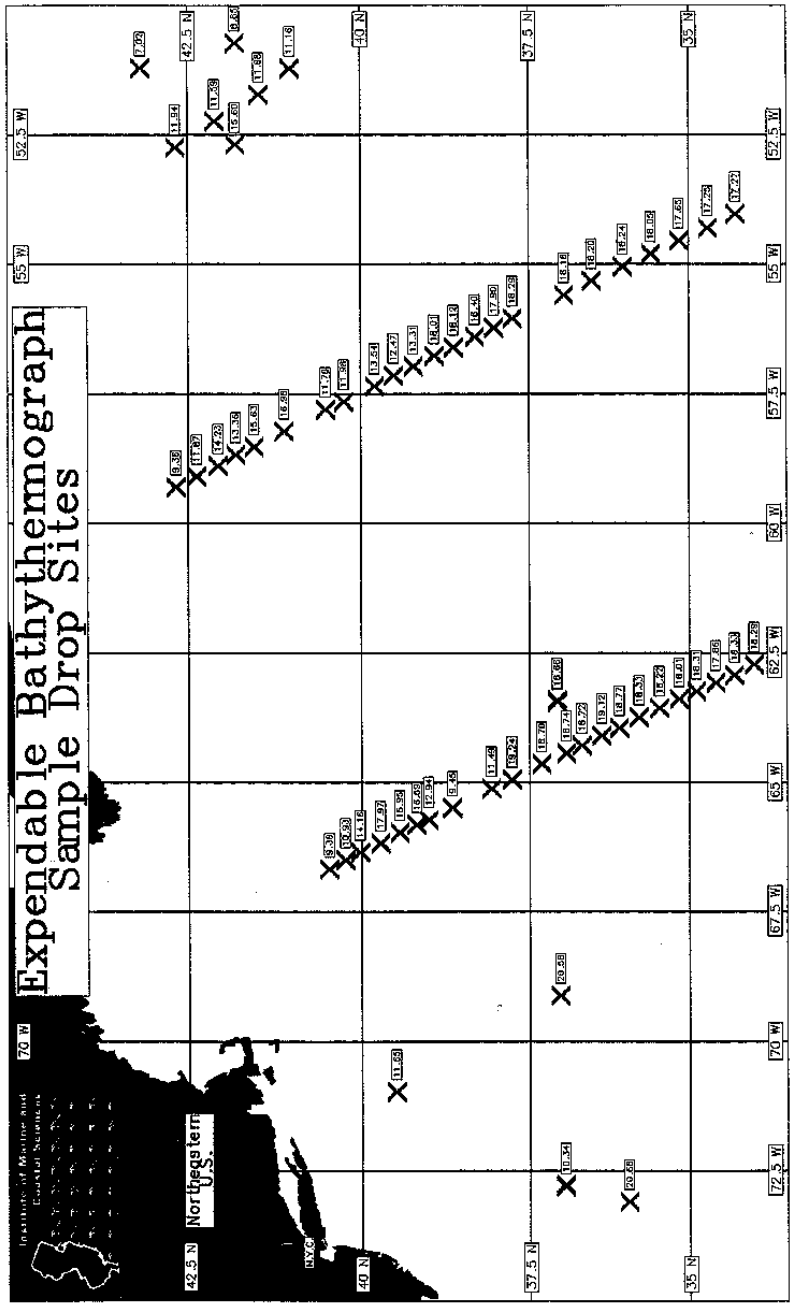

Figure 5: Sample expendable bathythermograph drop sites, with the temperature at 200 meter depth next to each drop site.

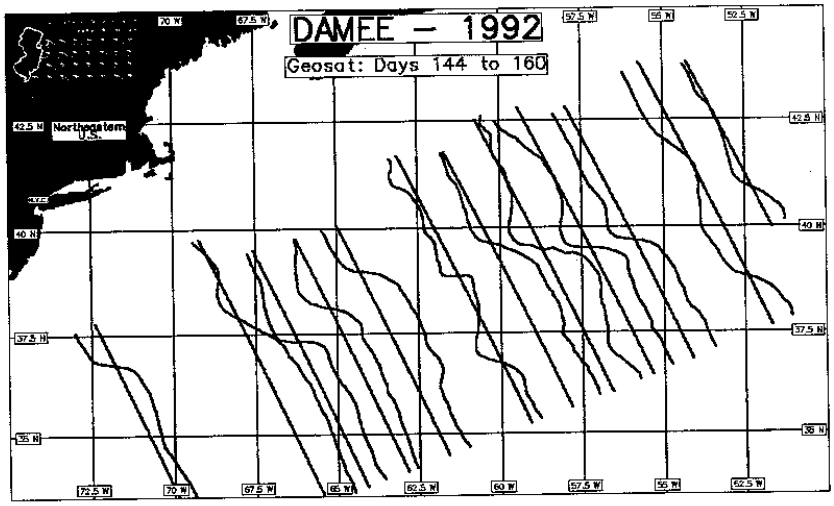

Figure 6: A 17 day composite of Geosat tracks and topographic variations during the first third of the study period.

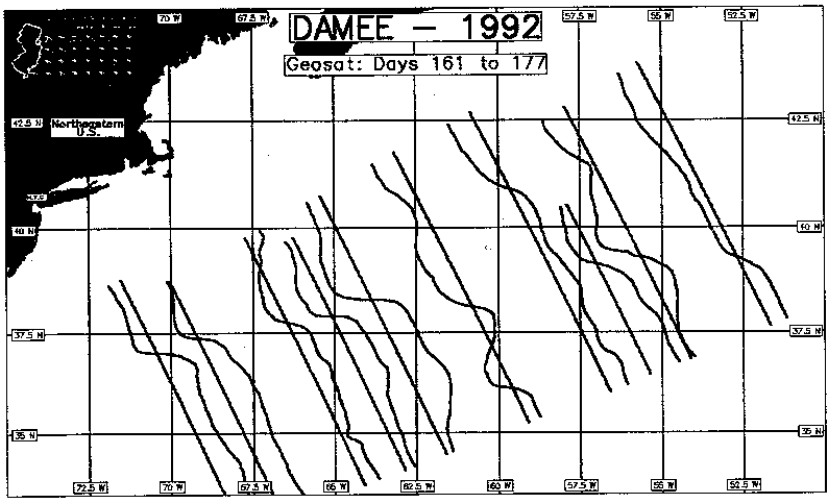

Figure 7: A 17 day composite of Geosat tracks and topographic variations during the second third of the study period.

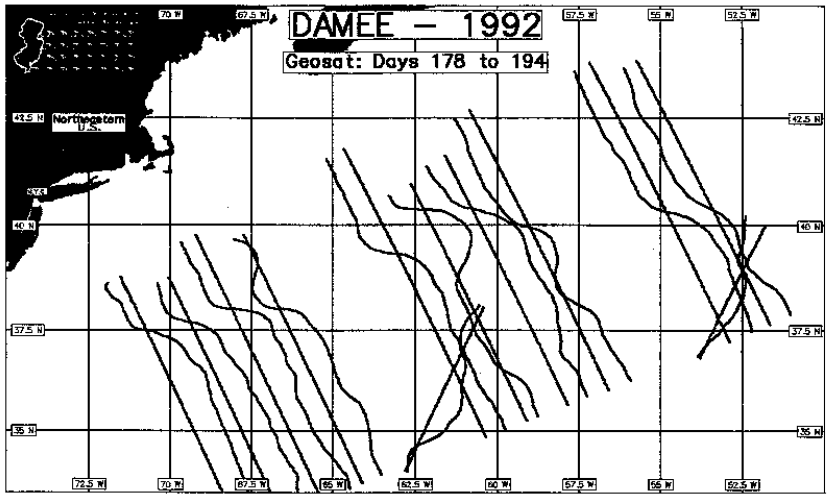

Figure 8: A 17 day composite of Geosat tracks and topographic variations during the last third of the study period.

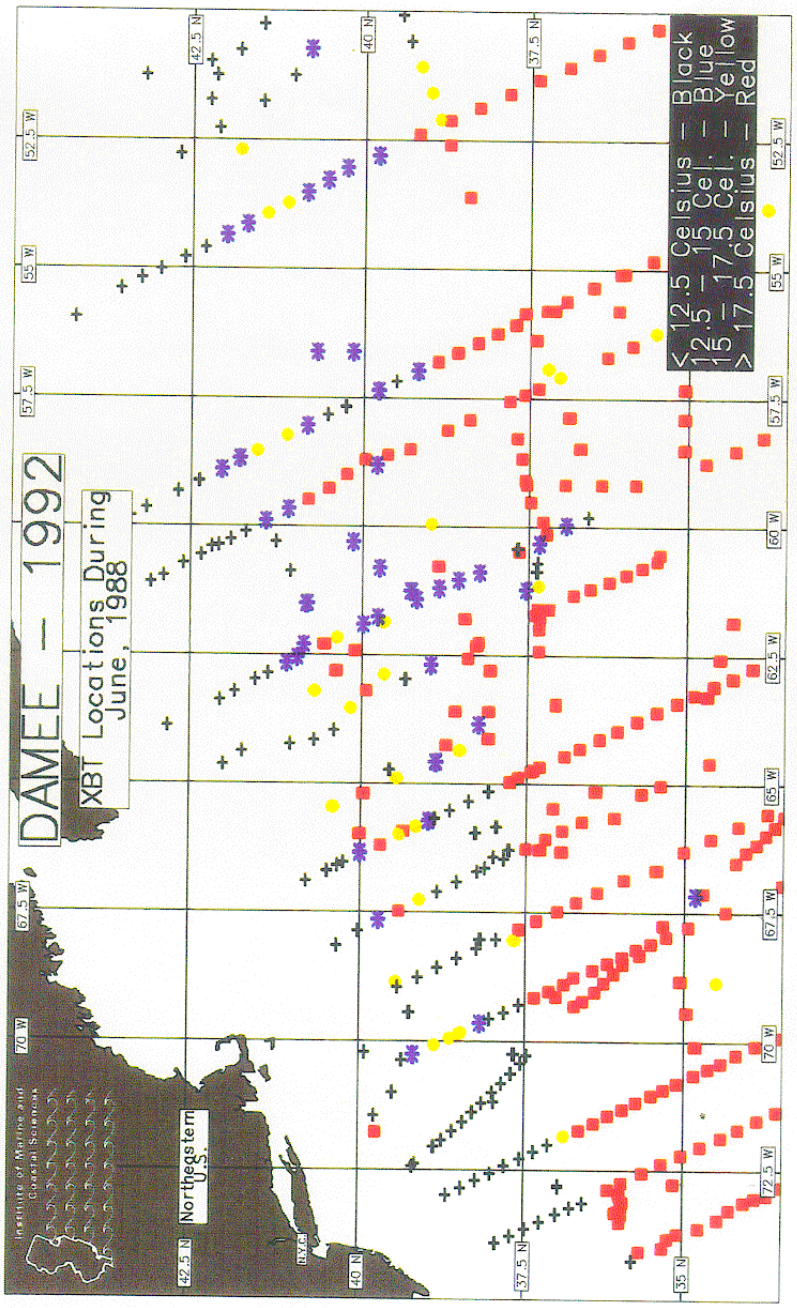

Figure 9: Location of all XBT data samples for the entire May 25 - July 4 study period.

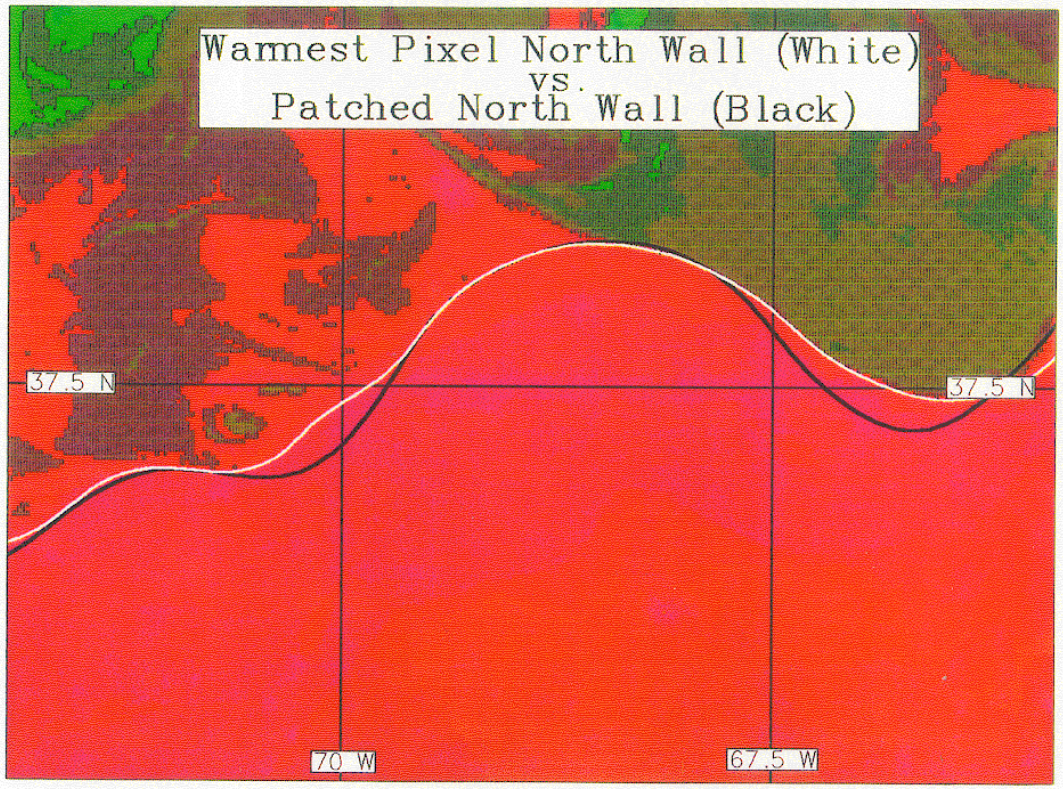

Figure 10: A section of a north wall derived from a warmest pixel composite (white) versus a section derived from a patched image (black). The source images for each composite were the same. The underlying image is the warmest pixel composite.

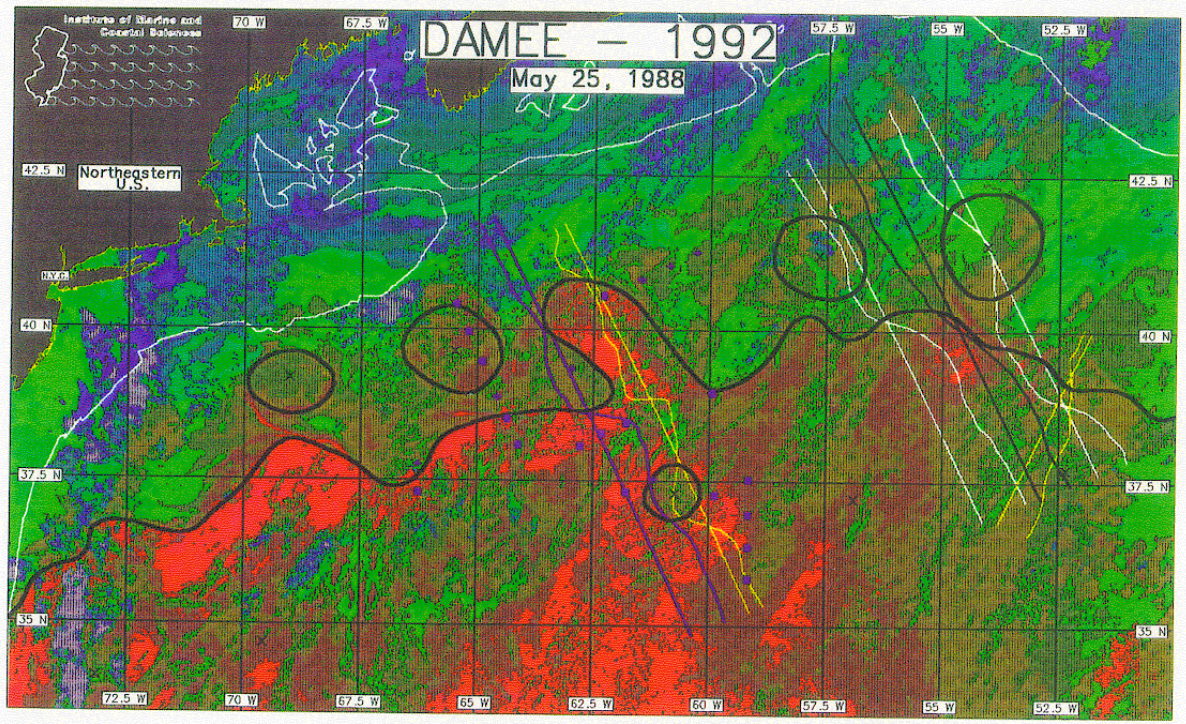

Figures 11-17: The completed maps of the Gulf Stream surface features. The thickest black lines represent the location of the north wall and visible rings. The AVHRR image, from the patched image technique, Geosat and XBT data are displayed as explained in the text. Black "x"'s mark the ring centers, including those that were interpolated. The 200 meter isobath is in white across the top of each map.

Figure 11: Completed map for May 25, 1988.

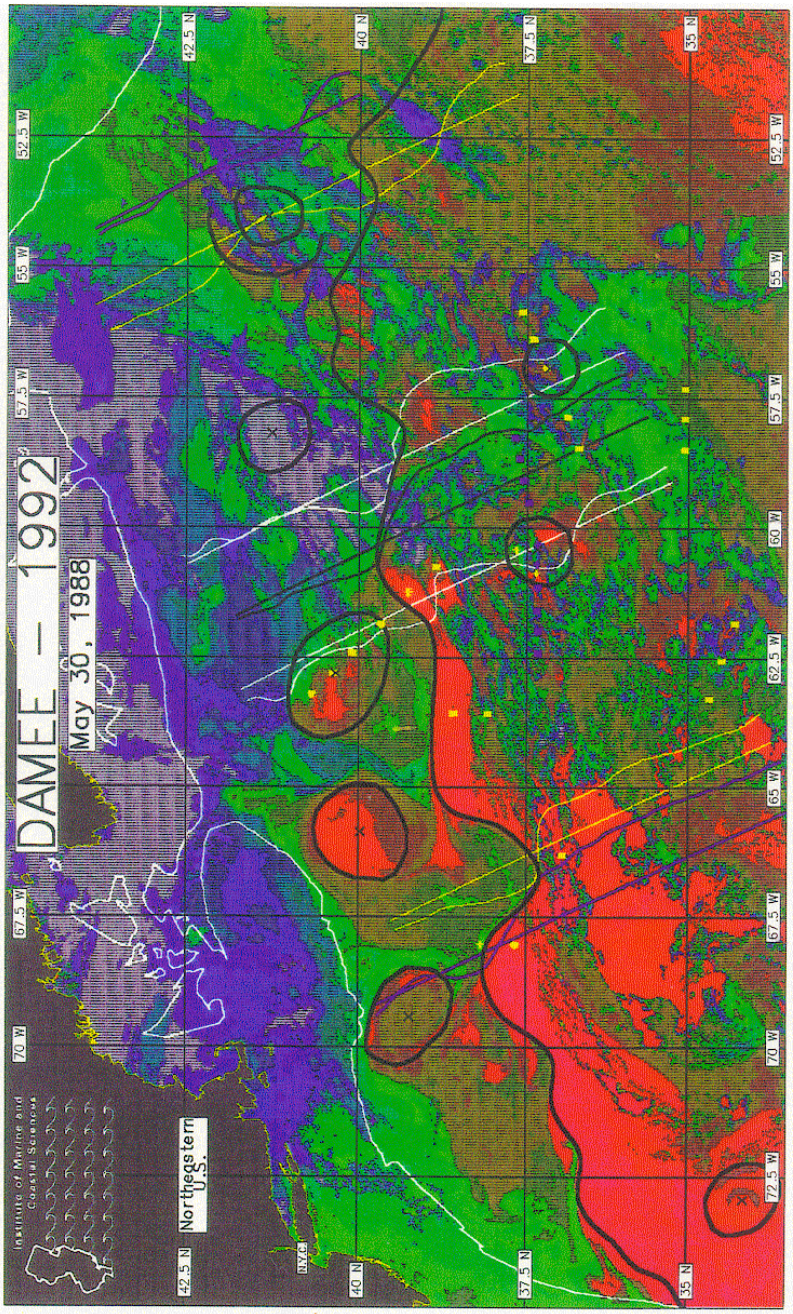

Figure 12: Completed map for May 30, 1988.

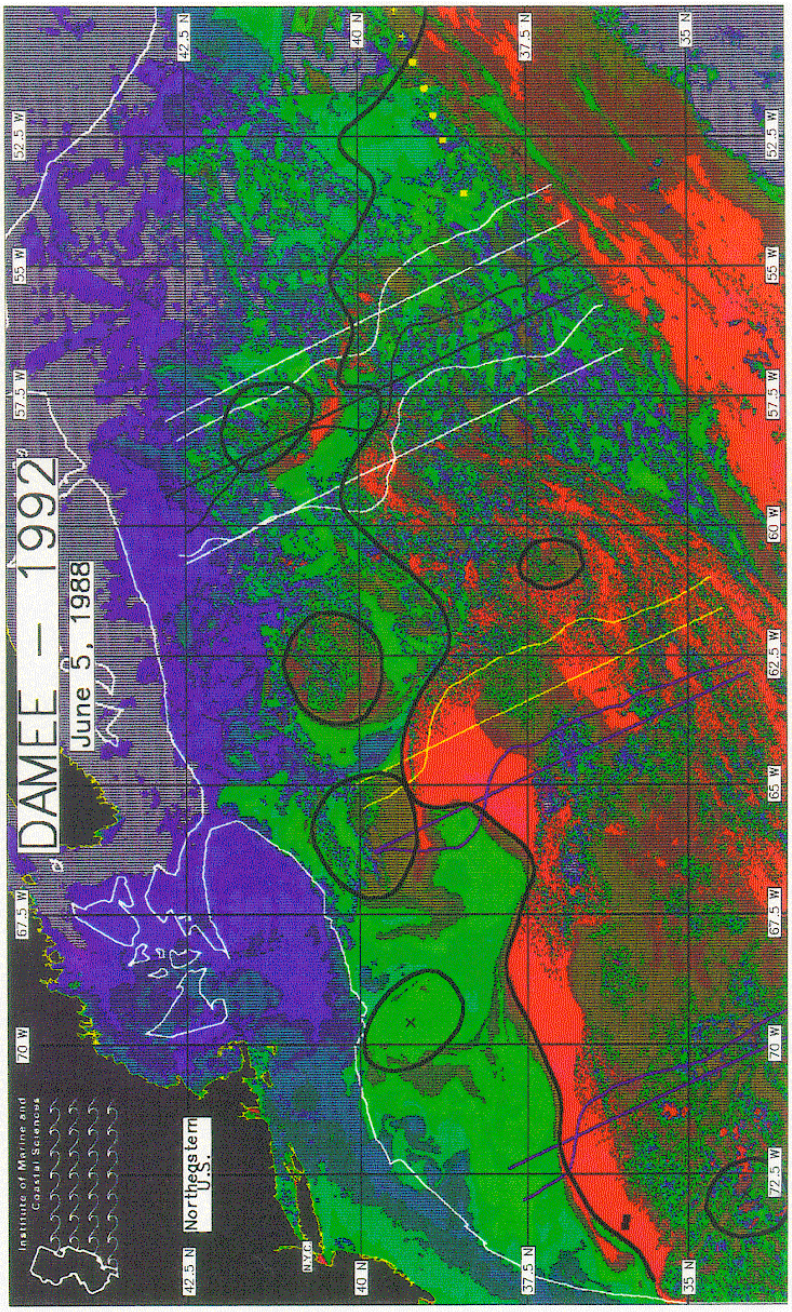

Figure 13: Completed map for June 5, 1988.

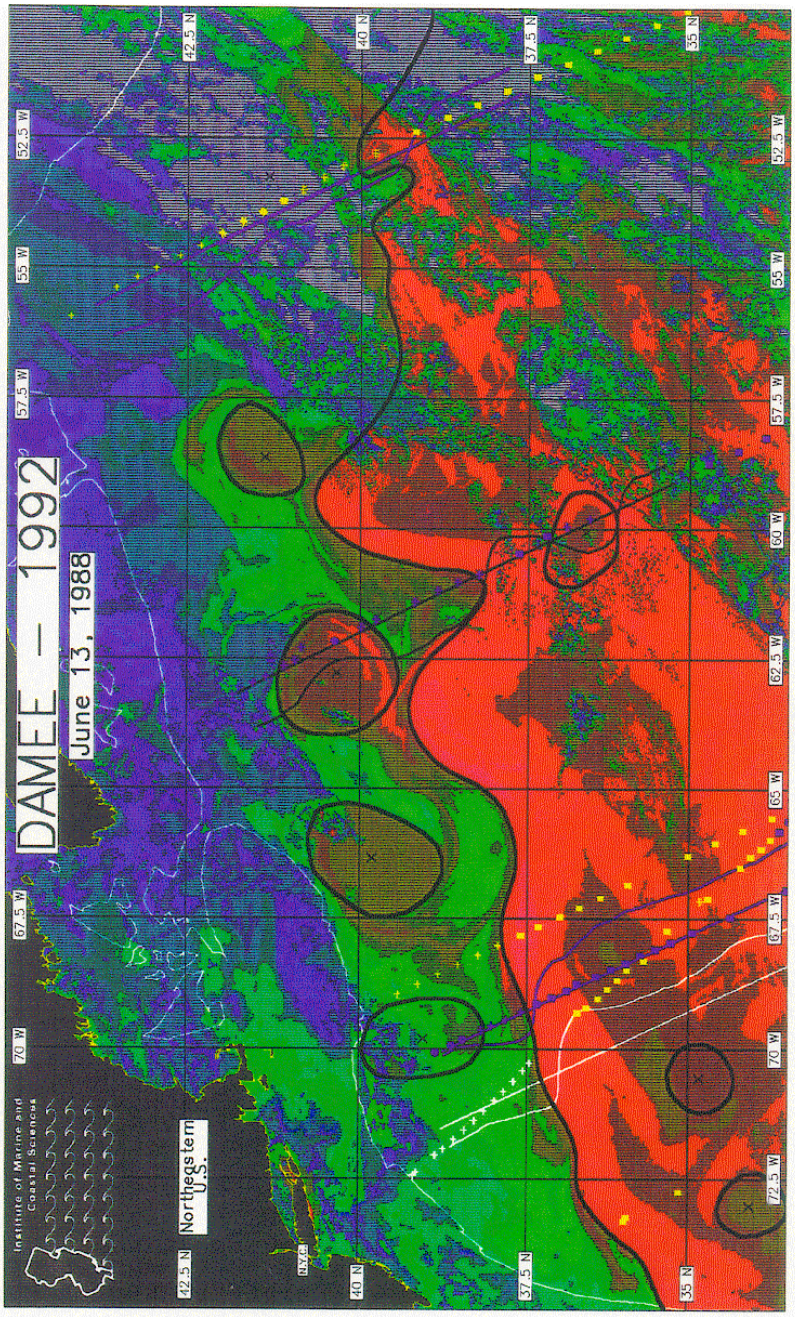

Figure 14: Completed map for June 13, 1988.

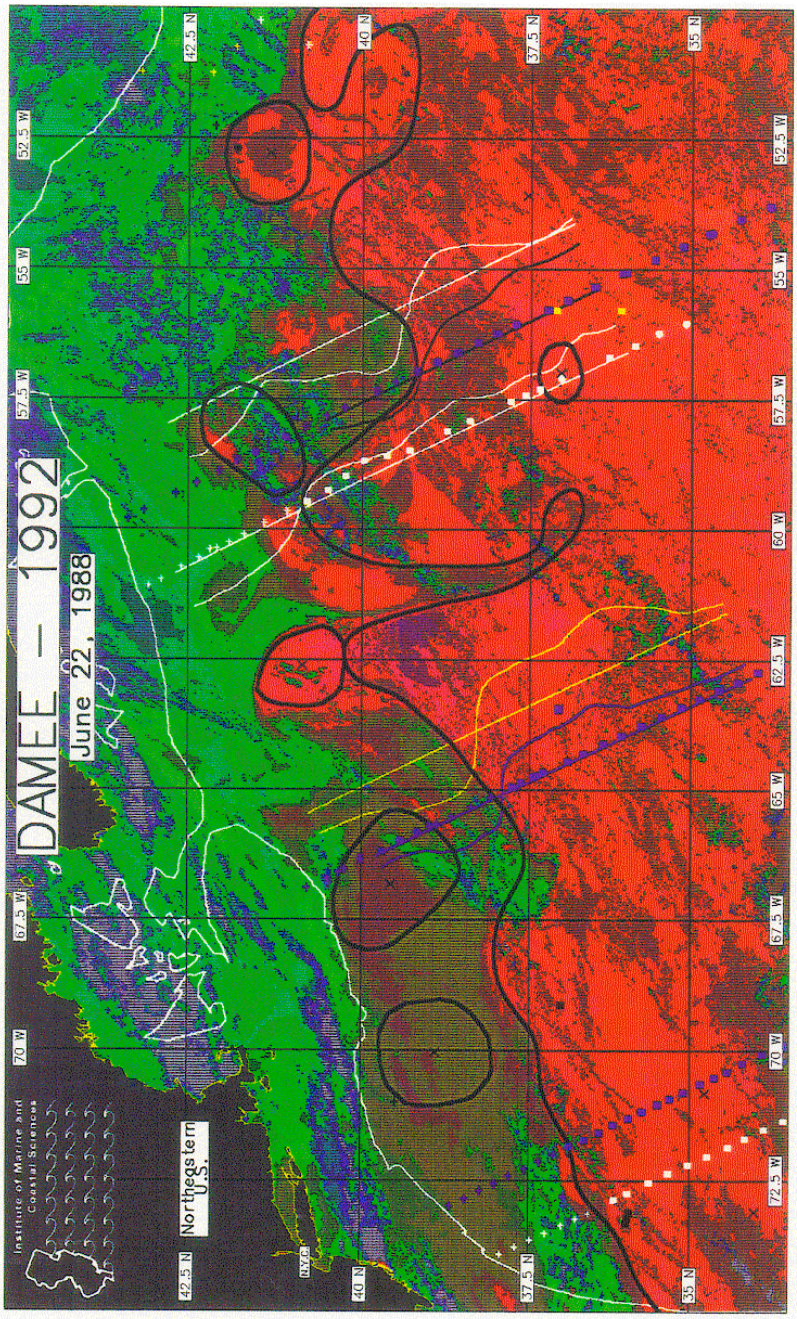

Figure 15: Completed map for June 22, 1988.

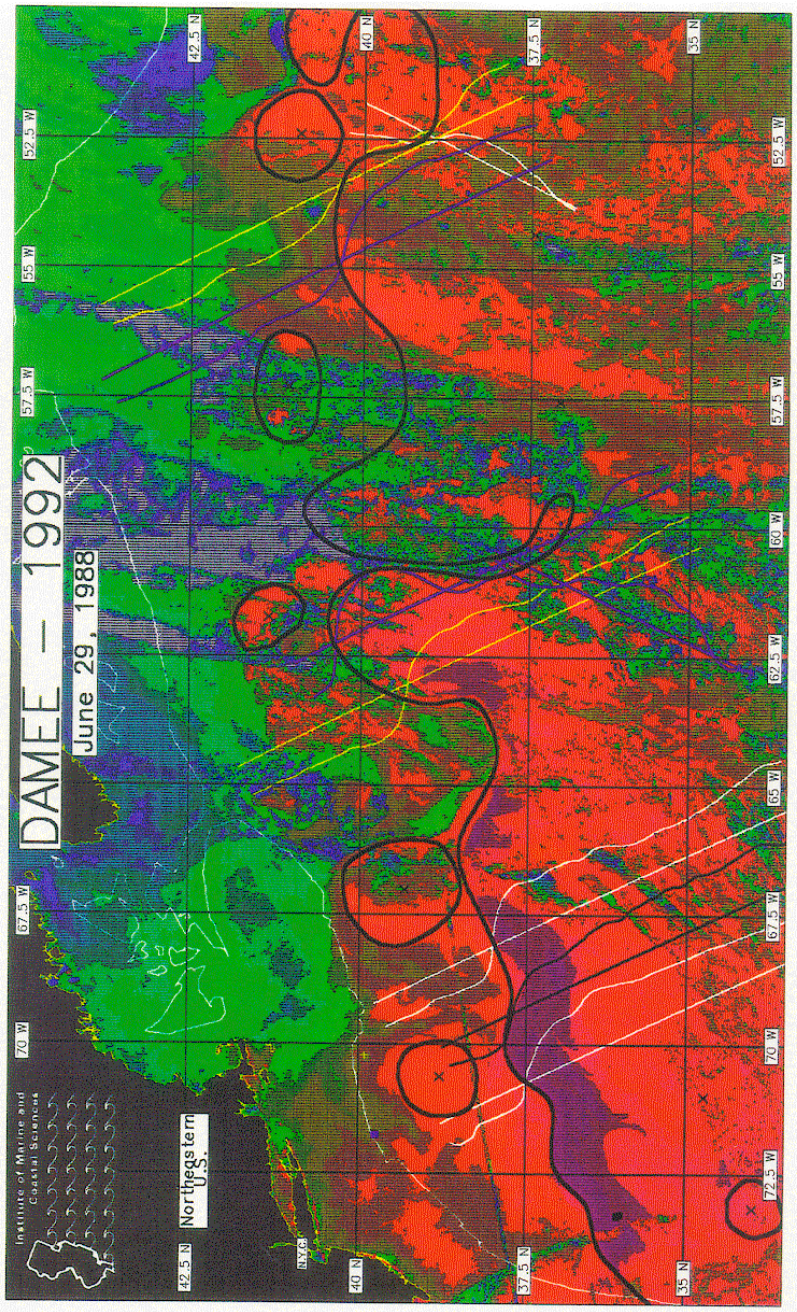

Figure 16: Completed map for June 29, 1988.

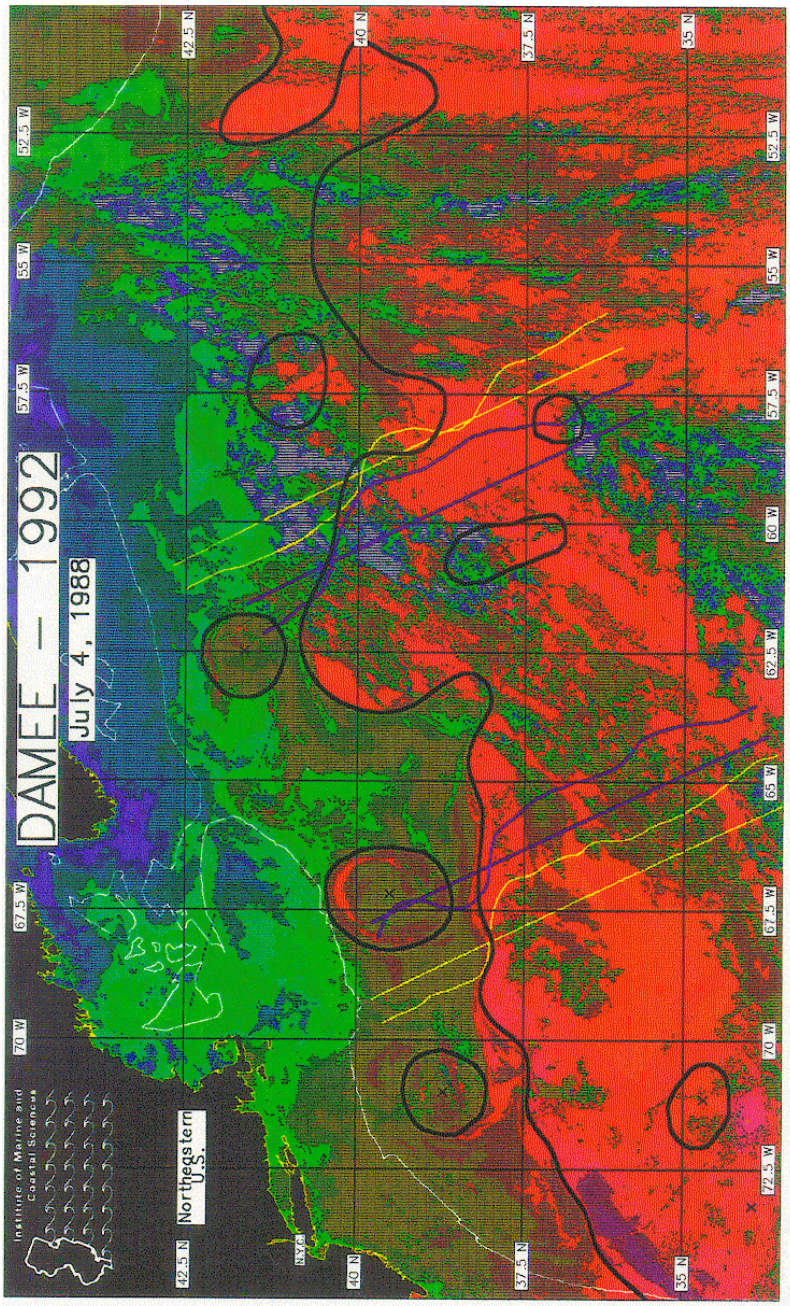

Figure 17: Completed map for July 4, 1988.

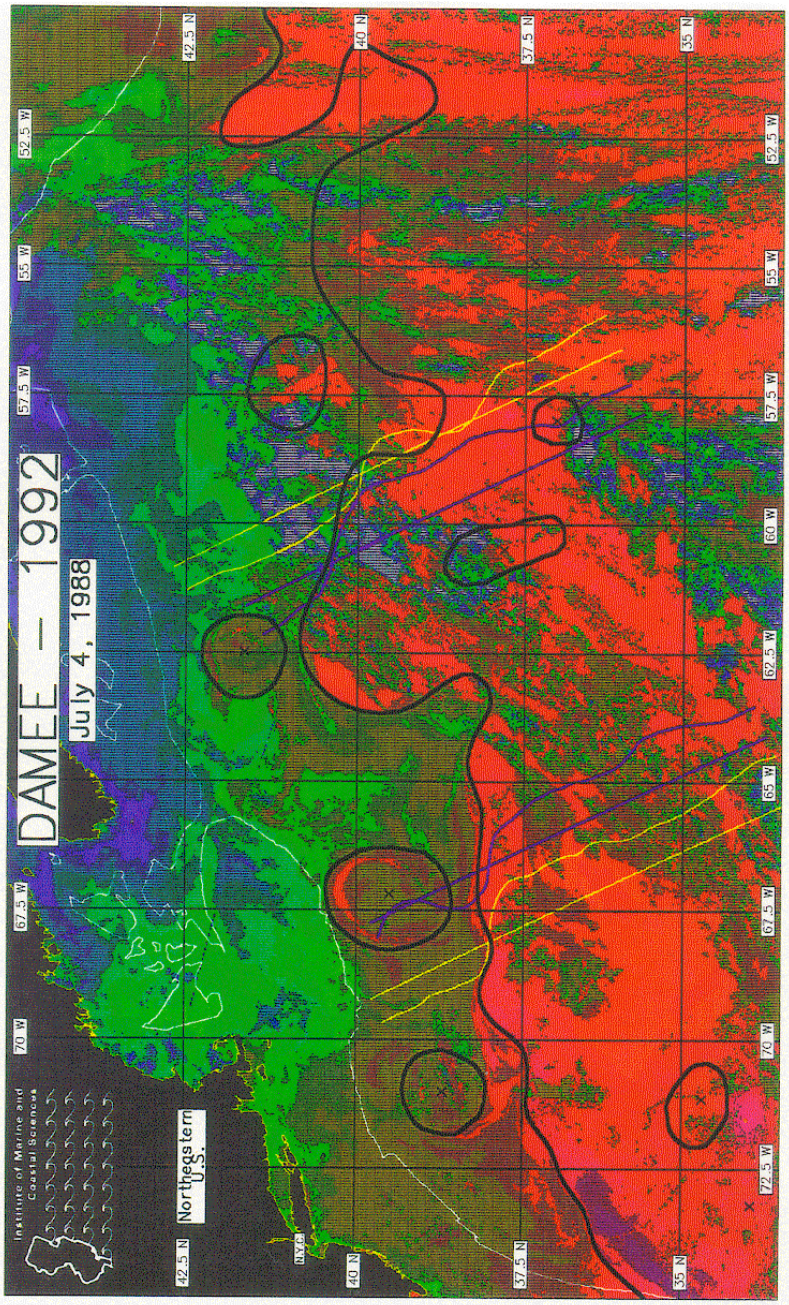

Figure 17: Completed map for July 4, 1988.

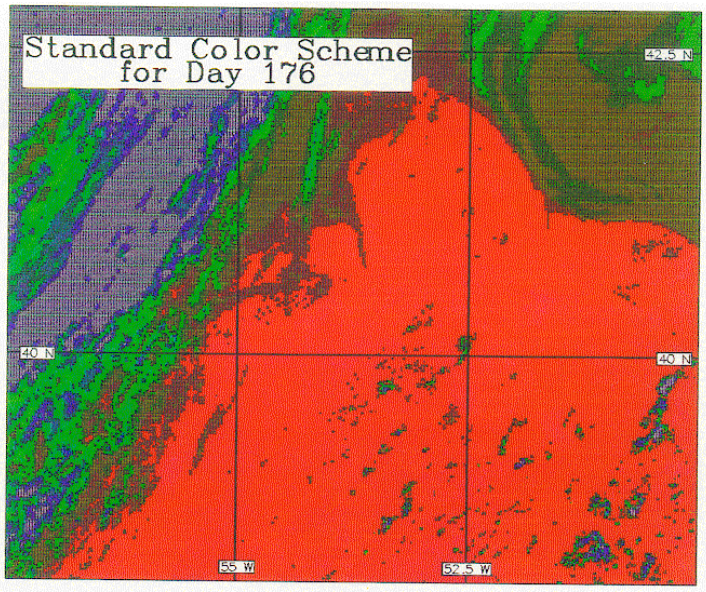

Figure 18a: A standard color wave applied to the AVHRR imagery.

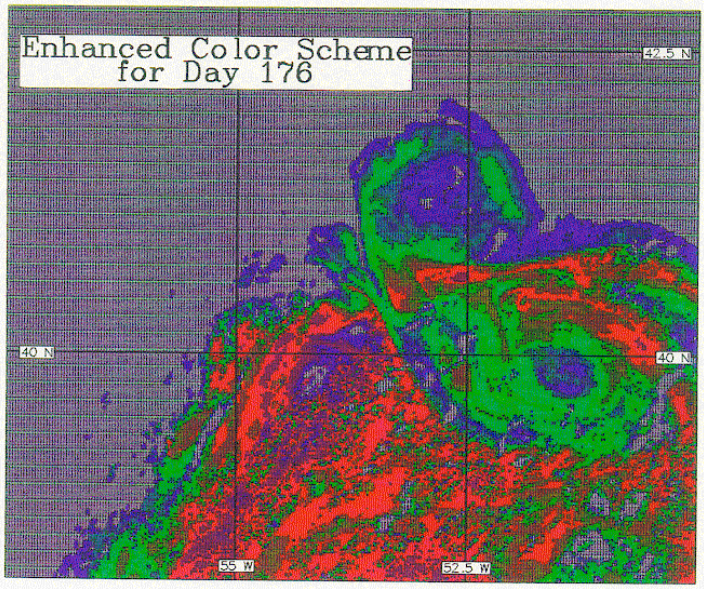

Figure 18b: An enhanced color wave applied to the same image as Figure 18a. Note the obvious surface features that are not visible in Figure 18a.

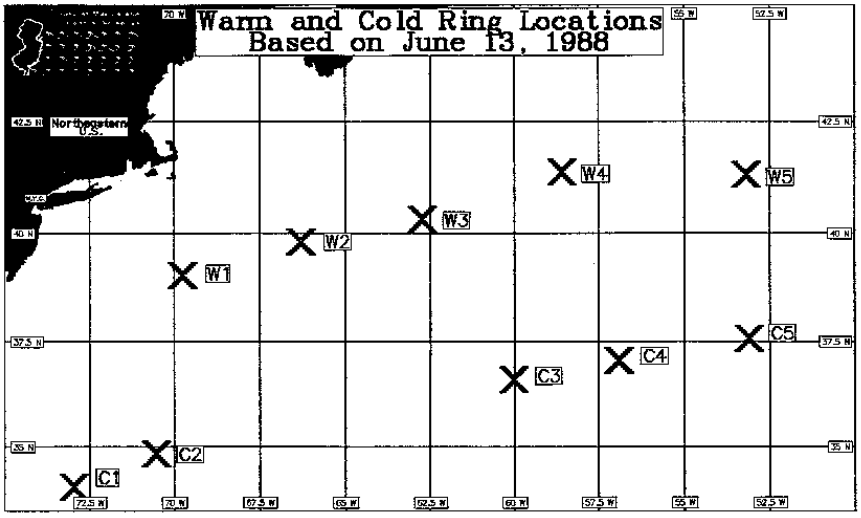

Figure 19: Warm and cold ring center locations for June 13, the central analysis day of the study period.

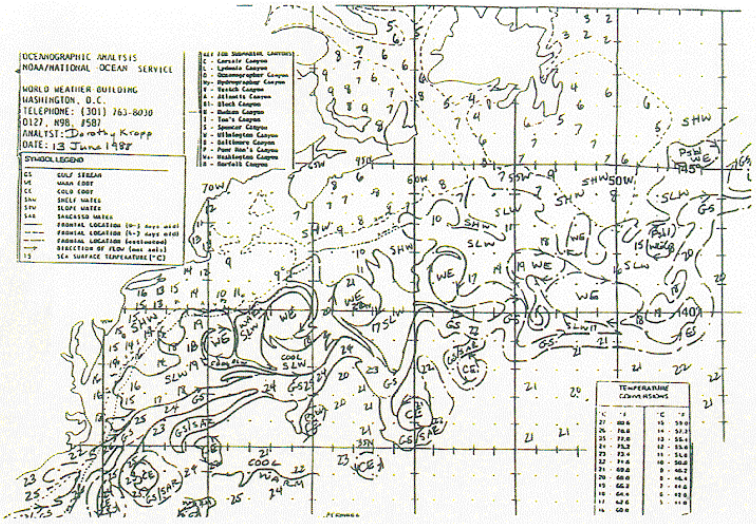

Figure 20: NOAA surface analysis of the Gulf Stream Meander and Ring Region for June 13, 1988.

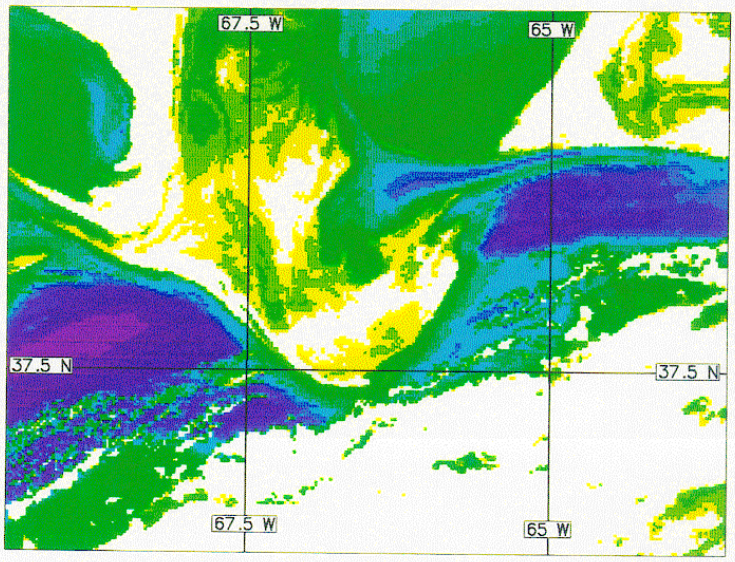

Figure 21a: An AVHRR image from day 151. Color schemes for this figure and Figure 20b are the same. The sea surface temperature signal of this figure at 38° N, 66° W is much weaker than Figure 20b because of cloud interference.

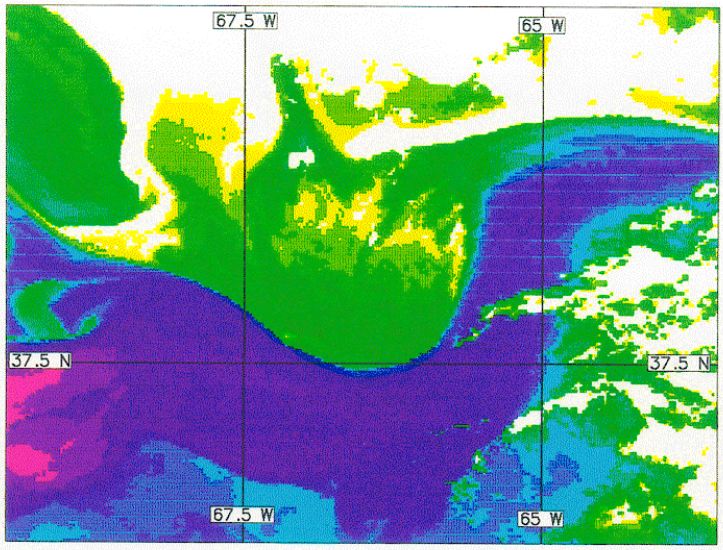

Figure 21b: AVHRR image from day 153.

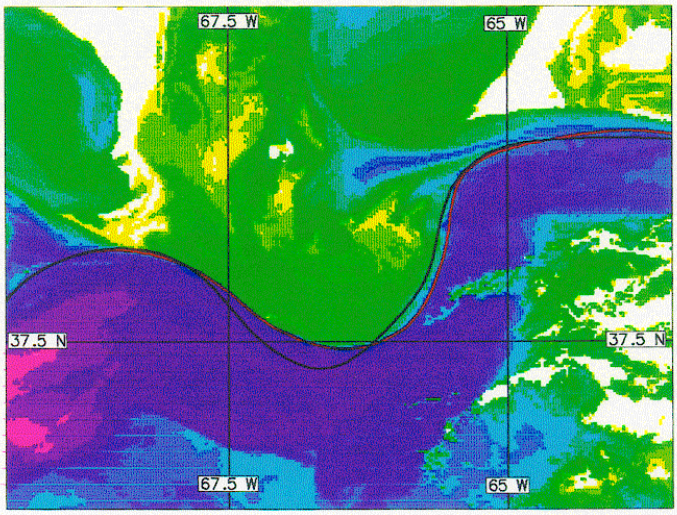

Figure 21c: A warmest pixel composite created from days 151 and 153. The black north wall is interpreted from the patched analysis whereas the red north wall was derived from the warmest pixel composite. The warmest pixel north wall is to the southeast of the patched wall at 38^{o}N, 66^{o}W because of the weak surface signature of the north wall on day 151 as compared to day 153.

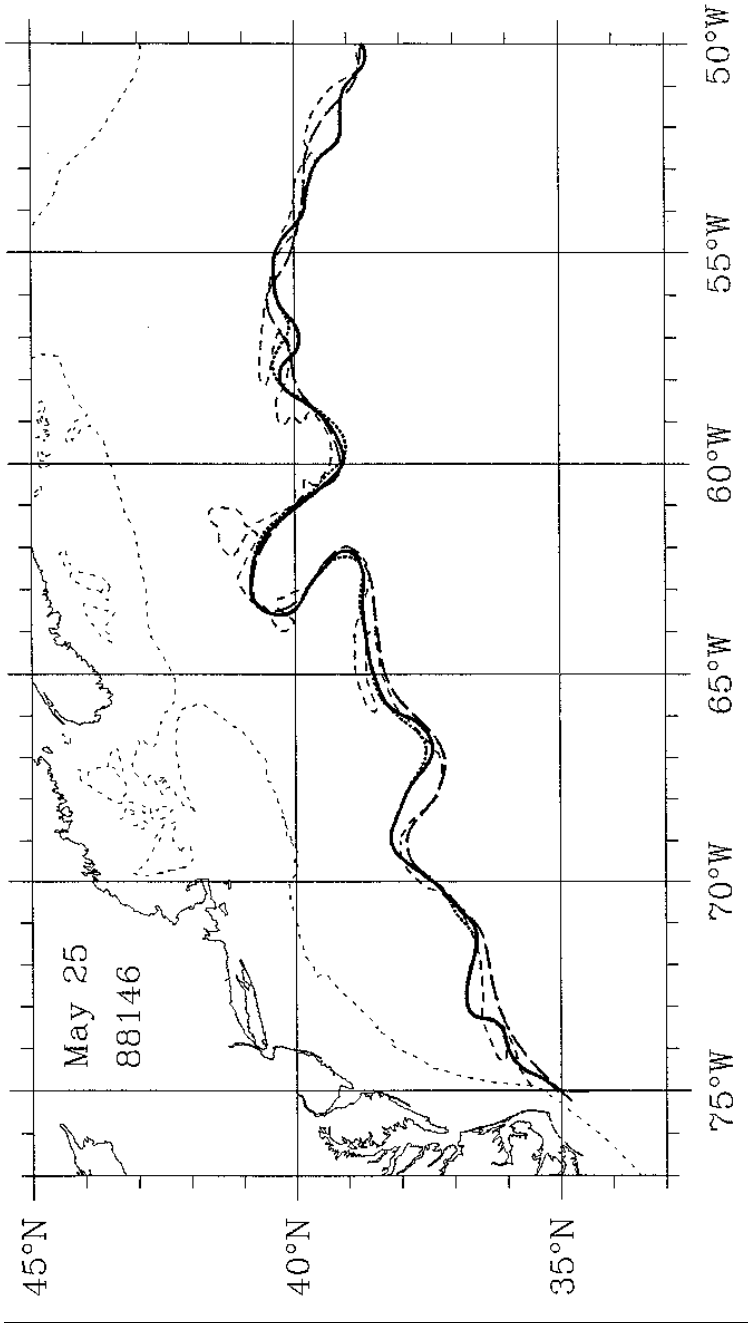

Figure 22: Gulf Stream north walls for May 25, 1988. Line patterns indicate the following sources for each analysis: Rutgers - solid, Harvard - long dash, NOAA - short dash, Warmest Pixel - dotted. All analyses are from Julian day 146.

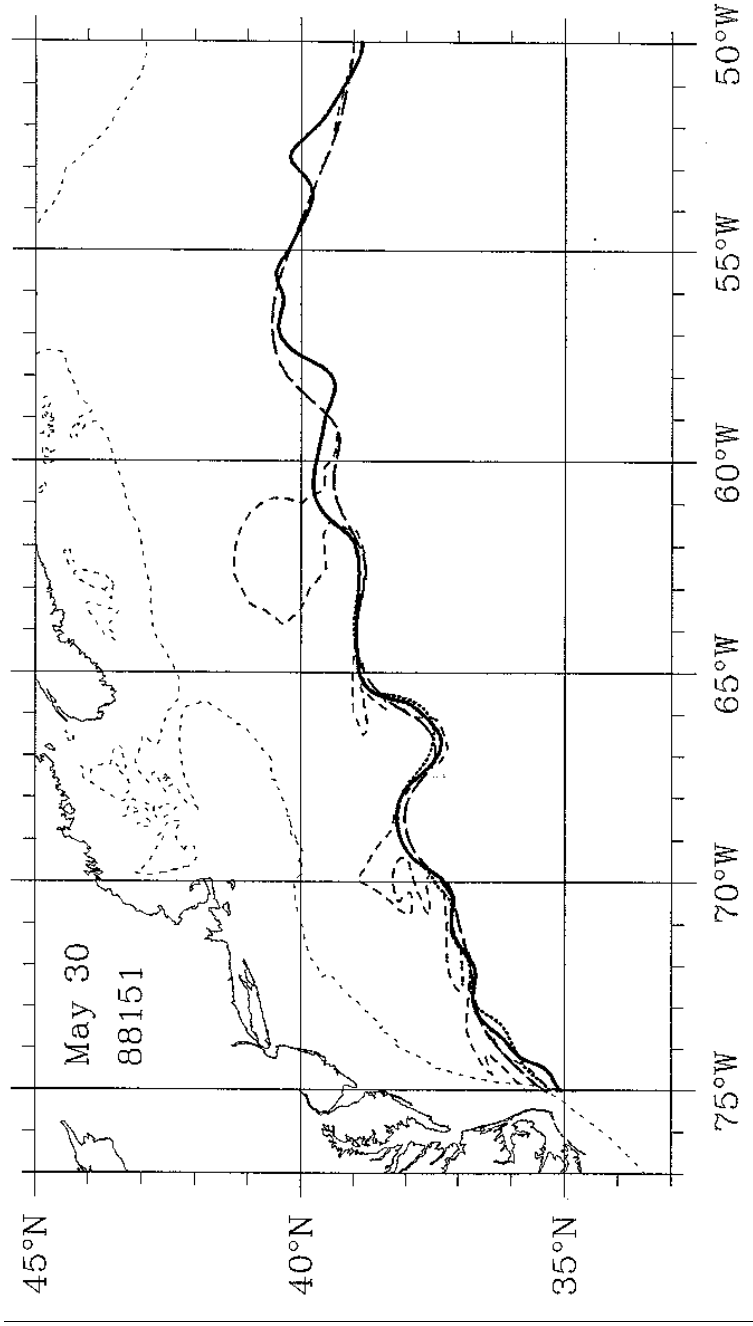

Figure 23: Gulf Stream north walls for May 30, 1988. Line patterns indicate the following sources for each analysis: Rutgers - solid, Harvard - long dash, NOAA - short dash, Warmest Pixel - dotted. The Harvard and NOAA analyses are from Julian day 153. The Rutgers analysis is from Julian day 151.

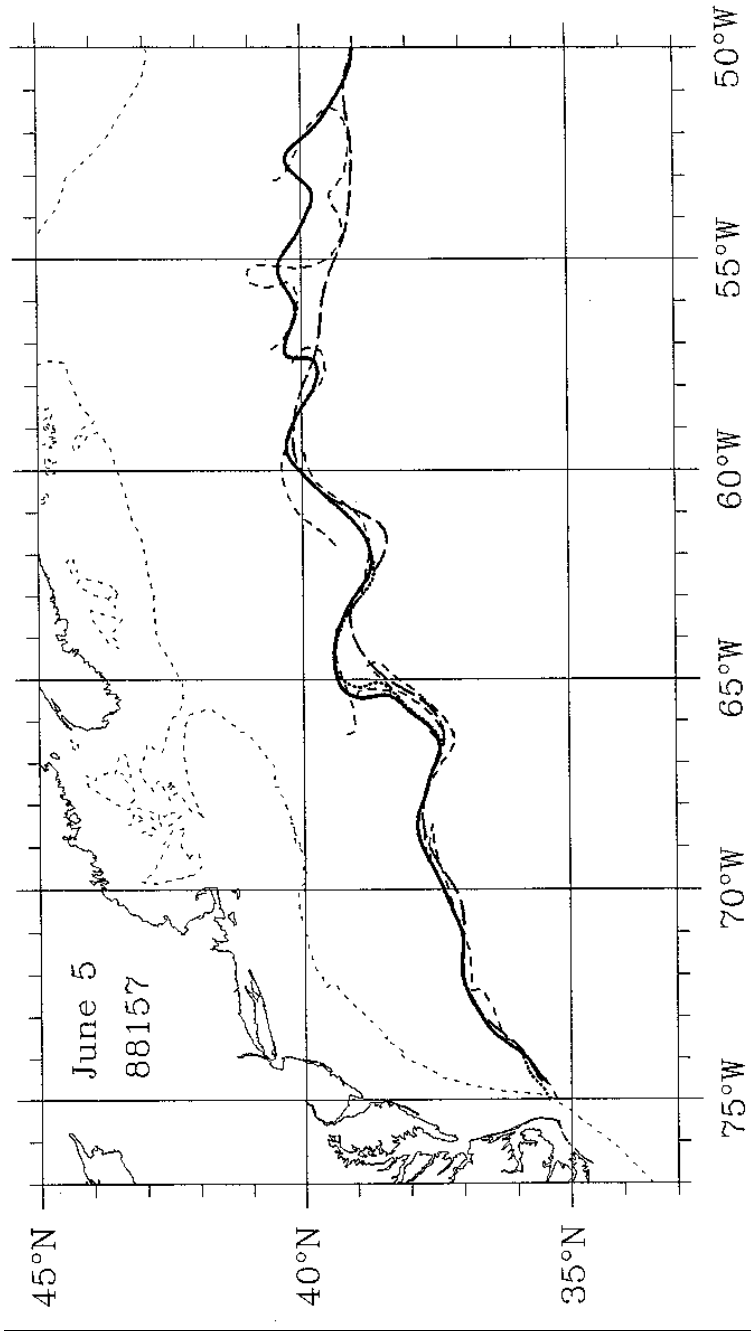

Figure 24: Gulf Stream north walls for June 5, 1988. Line patterns indicate the following sources for each analysis: Rutgers - solid, Harvard - long dash, NOAA - short dash, Warmest Pixel - dotted. The Harvard and NOAA analyses are from Julian day 160. The Rutgers analysis is from Julian day 157.

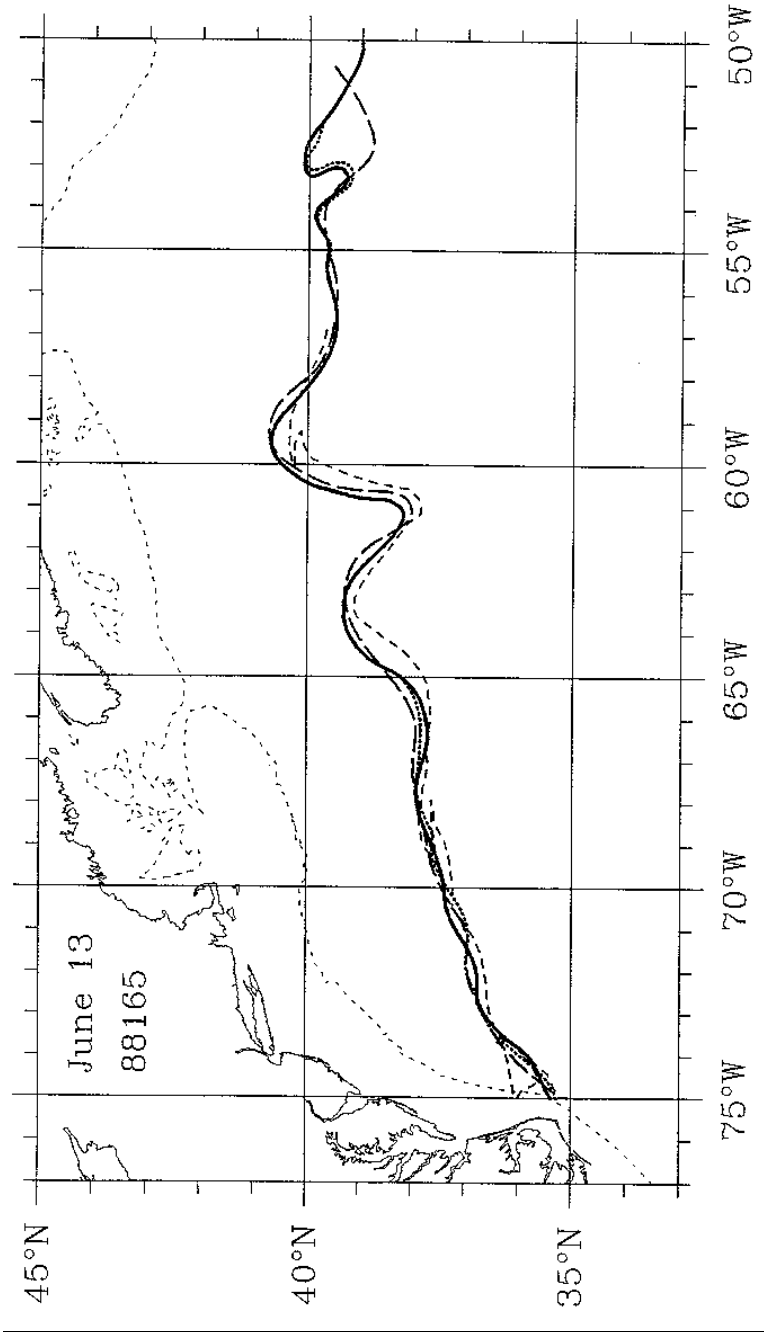

Figure 25: Gulf Stream north walls for June 13, 1988. Line patterns indicate the following sources for each analysis: Rutgers - solid, Harvard - long dash, NOAA - short dash, Warmest Pixel - dotted. The Harvard and NOAA analyses are from Julian day 167. The Rutgers analysis is from Julian day 165.

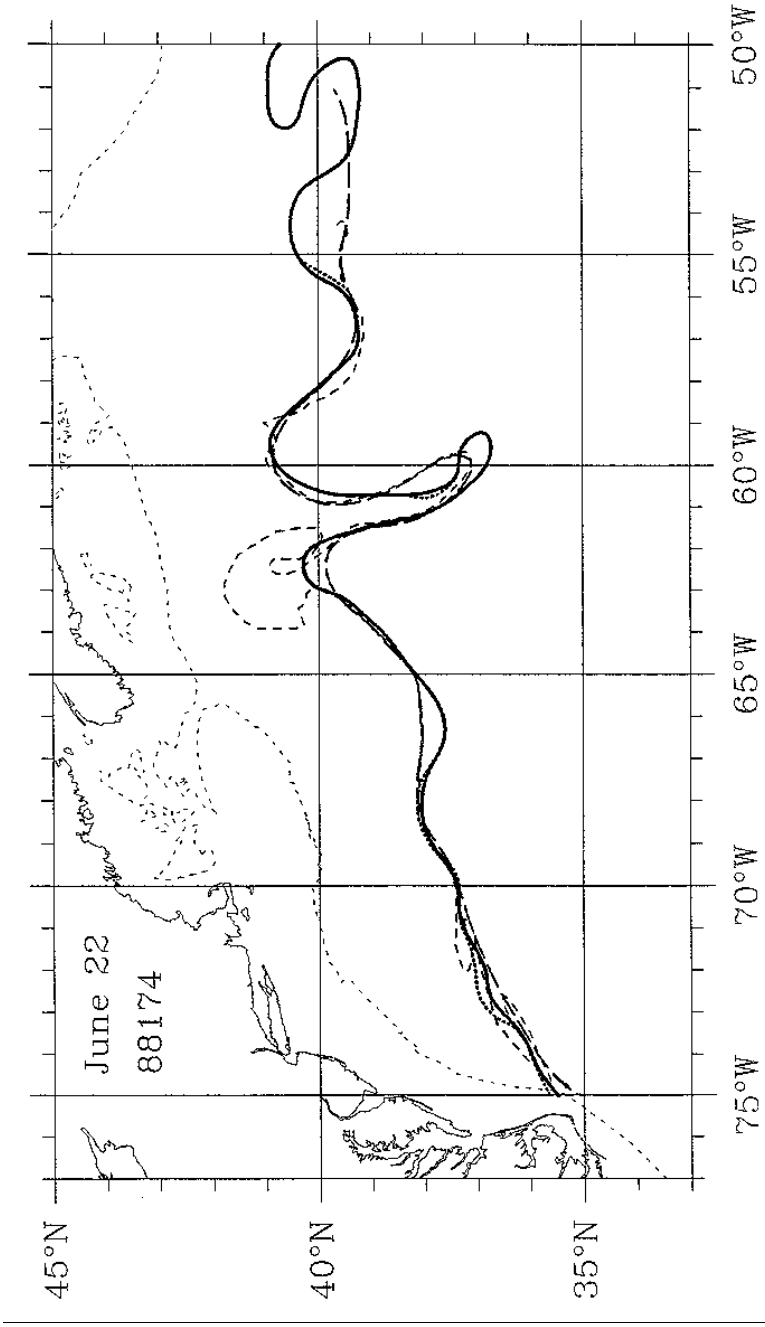

Figure 26: Gulf Stream north walls for June 22, 1988. Line patterns indicate the following sources for each analysis: Rutgers - solid, Harvard - long dash, NOAA - short dash, Warmest Pixel - dotted. The analyses are all from Julian day 174.

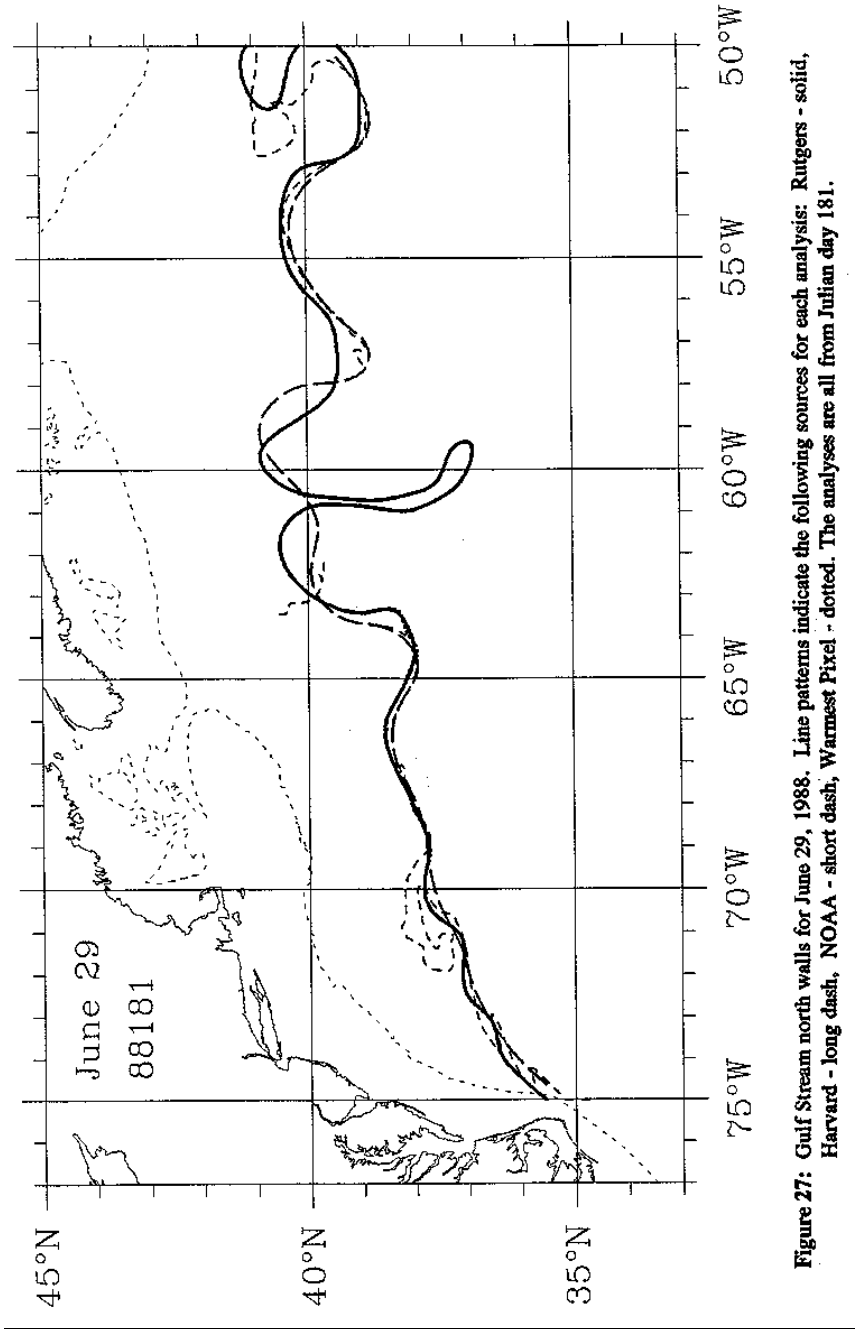

Figure 27: Gulf Stream north walls for June 29, 1988. Line patterns indicate the following sources for each analysis: Rutgers - solid, Harvard - long dash, NOAA - short dash, Warmest Pixel - dotted. The analyses are all from Julian day 181.

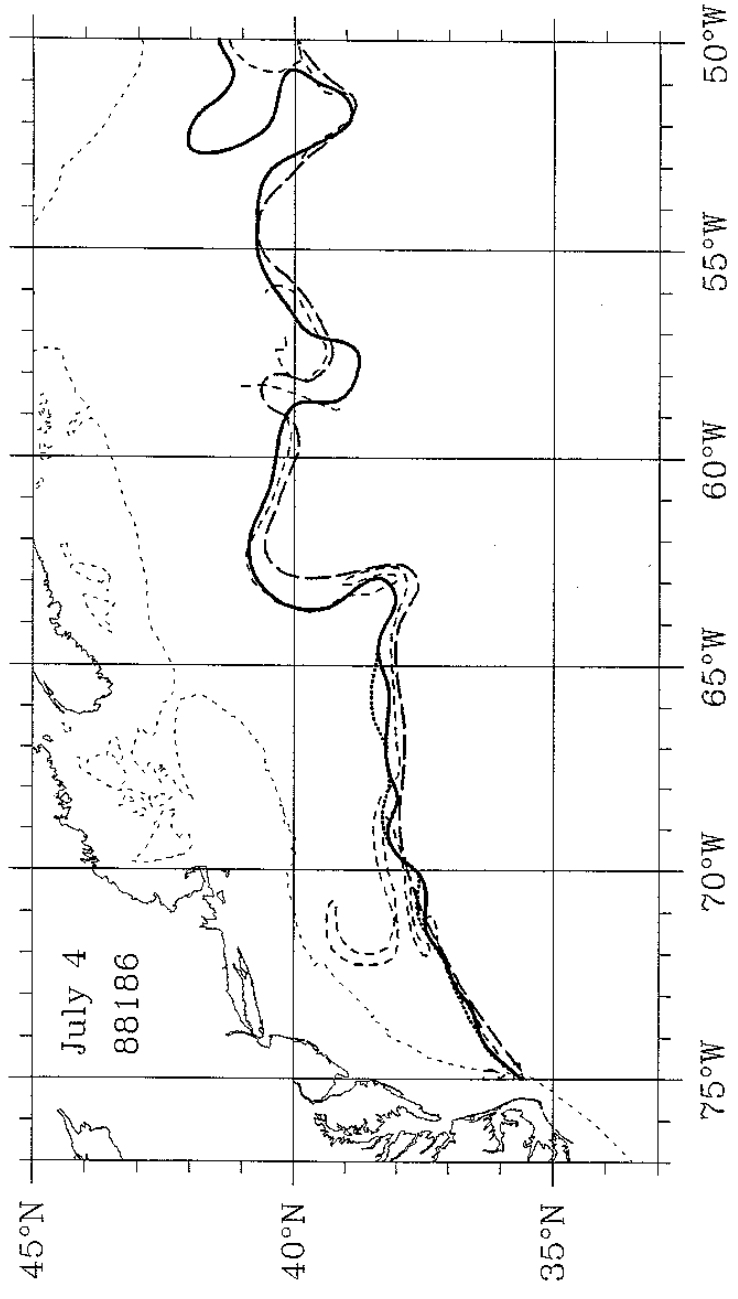

Figure 28: Gulf Stream north walls for July 4, 1988. Line patterns indicate the following sources for each analysis: Rutgers - solid, Harvard - long dash, NOAA - short dash, Warmest Pixel - dotted. The Harvard and NOAA analyses are from Julian day 188, while the Rutgers analysis is from Julian day 186.

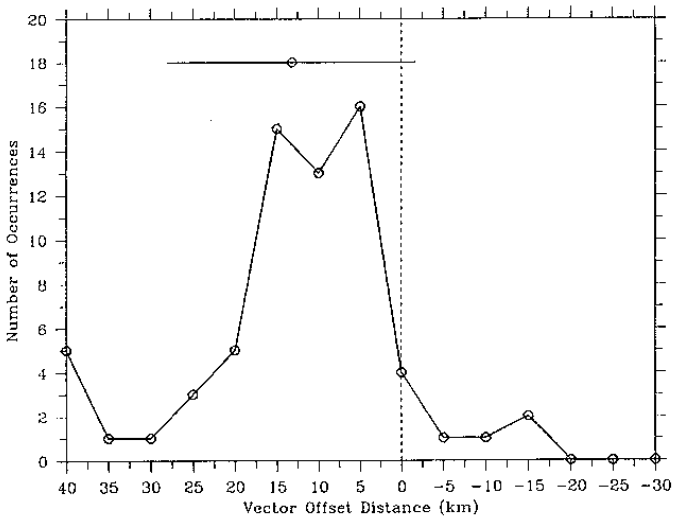

Figure 29: A histogram of vector distance offsets between the Geosat altimeter derived maximum velocity axis and the AVHRR derived surface north wall. The average and standard deviation are indicated by the circle and line at the top of the figure. Positive values indicate the AVHRR derived north wall is north of the Geosat axis.

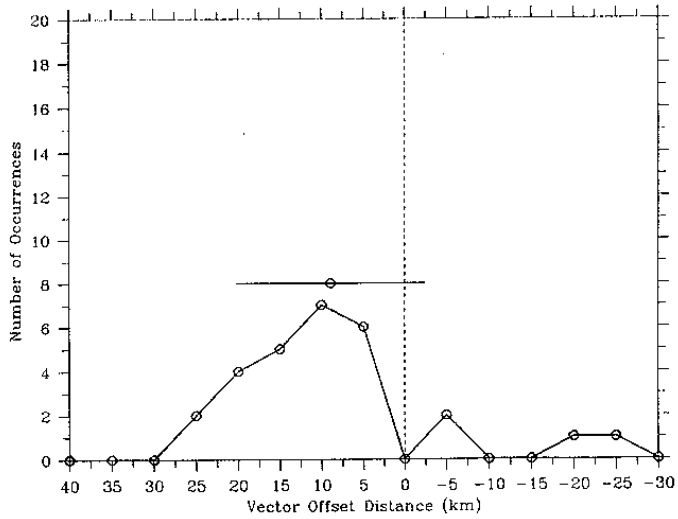

Figure 30: A histogram of the vector distance offsets between the sub-surface north wall interpolated from along-Geosat-track XBT drops and the Geosat derived maximum velocity axis. The average and standard deviation are indicated by the circle and line above the histogram. Positive values indicate the XBT subsurface wall is north of the Geosat axis.

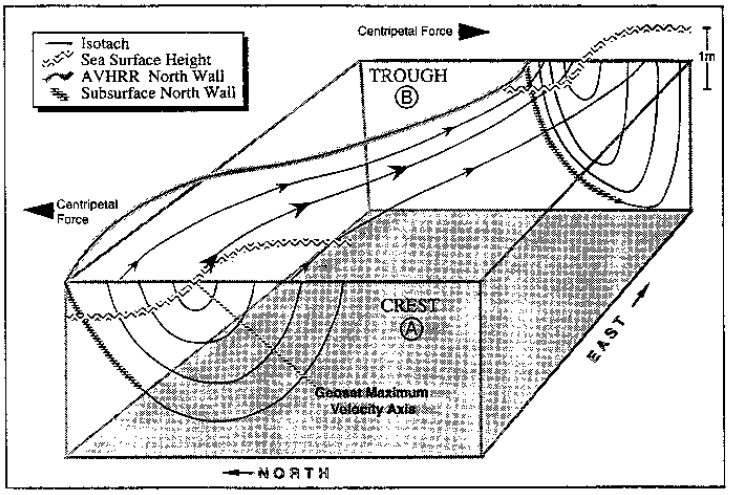

Figure 31: The Jet Stream wave pattern in the atmosphere, which also can be used to illustrate the effects of centripetal acceleration on the Gulf Stream. Point A is a typical meander crest cross-section, whereas point B is a typical meander trough cross-section. Note that centripetal acceleration results in a wider Stream and shallower sloping isotachs at point A and a narrower Stream and steeper sloping isotachs at point B (Newton, 1978).

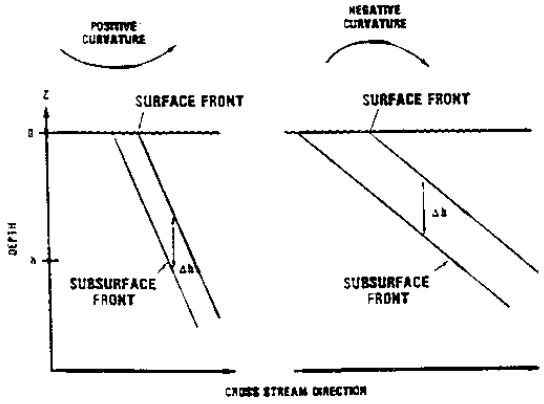

Figure 32: Cross-stream frontal slope and the normal separation between isopycnals making up the front. The difference in slope between positive (trough) and negative (crest) curvature is highlighted (Horton, 1986).

References

Aronoff, Stan, 1989. Geographic Information Systems: A Management Perspective, Ottawa, Canada: WDL Publications, pp. 293.

Auer, S.J., 1980. "New Daily Oceanographic Analyses." Gulfstream, 6: 3-7.

Bearman, Gerry (ed.), 1989. Ocean Circulation. Oxford: Pergamon Press, pp. 236.

Calman, Jack, 1987. "Introduction to Sea-Surface Topography from Satellite Altimetry." Johns Hopkins APL Technical Digest, 8:2:206-211.

Clancy, M.P., P.A. Phoebus, K.D. Pollak, 1990. "Operational Global Scale Ocean Thermal Analysis System." Journal of Atmospheric and Oceanic Technology, 7(2): 233-254.

Clark, Jenifer, 1988. "East Coast Ocean Features." Oceanographic Monthly Summary, 8(5,6,7), 2 pp.

Cornillon, P., D. R. Watts, 1987. "Satellite Thermal Infrared and Inverted Echo Sounder Determinations of the Gulf Stream Northern Edge." Journal of Atmosphere and Oceanic Technology, 4:712-723.

Cressy, Peter, 1986. "Naval Oceanography and Ocean Prediction." Ocean Prediction Workshop: 1986. A Status and Prospectus Report on the Scientific Basis and the Navy's Needs, 494 pp.

DAMEE, 1991. DAMEE News and Notes, Institute for Naval Oceanography, 1(1). pp.2.

Glenn, Scott M., Allan Robinson, Michael Spall, 1987. "Recent Results from the Harvard Gulf Stream Forecasting Program." Oceanographic Monthly Summary, 7:4:3, 12-13.

Glenn, Scott M., G. Z. Forristall, P. Cornillion, G. Milkowski, 1990. "Observations of Gulf Stream Ring 83-E and Their Interpretation Using Feature Models." Journal of Geophysical Research, 95:C8:13043-13063.

Glenn, Scott M., David L. Porter, Allan R. Robinson, 1991a. "A Synthetic Geoid Validation of Geosat Mesoscale Dynamic Topography in the Gulf Stream Region." Journal of Geophysical Research, 96:C4:7145-7166.

Glenn, Scott M., Dick Crout, Louise Perkins, 1991b. "Comparison of Gulf Stream Forecast Model Initialization and Verification Analyses." Institute for Naval Oceanography, TM-6:1-38.

Glenn, Scott M., Allan R. Robinson, 1991. "A Continuous Temperature and Salinity Model Across the Gulf Stream." Harvard Open Ocean Model Reports, No. 38.

Hepplewhite, C., 1989. "Remote Observation of the Sea Surface and Atmosphere: The Ocean Skin Effect." International Journal of Remote Sensing, 10 (4-5): 801-810.

Horton, Charles W., 1986. "Modulation of Gulf Stream Surface-Subsurface Frontal Separation by path Curvature." Journal of Physical Oceanography, 17: 596 - 603.

Lee, T., P. Cornillion, 1991. "Propagation and Growth of Gulf Stream Meanders." AGU-MSA Spring Meeting 1991 Abstract Volume, p. 148.

Lybanon, Matthew, Richard L. Crout, 1987. "The NORDA Geosat Ocean Applications Program." Johns Hopkins APL Technical Digest, 8:2: 212-218.

Lybanon, Matthew, Richard L. Crout, Conrad H. Johnson, Pavel Pistek, 1990. "Operational Altimeter-Derived Oceanographic Information: The NORDA Geosat Ocean Applications Program." Journal of Atmospheric and Oceanic Technology, 7:3:357-376.

MacArthur, Paul C., Paul C. Marth, Joseph G. Wall, 1987. "The Geosat Radar Altimeter." Johns Hopkins APL Technical Digest, 8:2: 176-181.

McConathy, Donald R., Charles C. Kilgus, 1987. "The Navy Geosat Mission: An Overview." Johns Hopkins APL Technical Digest, 8:2:170-175.

Mitchell, J.L., J. M. Dastugue, 1990. "The Estimation of Geoid Profiles in the North West Atlantic from Simultaneous Satellite Altimetry and Airbourne Expendable Bathythermograph Sections." Journal of Geophysical Research, 95(C10): 17965-17977.

Mooers, C.N.K., A.R. Robinson, J.D. Thompson, (co-conveners), 1986. Ocean Prediction Workshop: 1986, A Status and Prospectus Report on the Scientific Basis and the Navy's Needs, Department of the Navy (Office of Naval Research), 494 pp.

Newton, Chester W., 1978. "Fronts and Wave Disturbances in Gulf Stream and Atmospheric Jet Stream." Journal of Geophysical Research, 83: C9: 4697 - 4706.

Onorati, Roger, 1986. "The Commanding Officer's Views of INO and Charge to OPW86." Ocean Prediction Workshop: 1986. A Status and Prospectus Report on the Scientific Basis and the Navy's needs, 494 pp.

Porter, David, Allan R Robinson, Scott M. Glenn, Ella B. Dobson, 1989. "The Synthetic Geoid and the Estimation of Mesoscale Absolute Topography from Altimeter Data." Johns Hopkins APL Technical Digest, 10:4:369-379.

Porter, David, Scott M. Glenn, Ella B. Dobson, Allan R. Robinson, 1990. "GEOSAT: A U.S. Navy Spaceborne Altimeter." Oceanus, 33:4:50-57.

Robinson, Allan R., Michael A. Spall, Wayne G. Leslie, Leonard J. Walstad, Dennis J. Mcgillicuddy, 1987a. "Gulfcasting: Dynamical Forecast Experiments for Gulf Stream Rings and Meanders: November 1985 to June 1986." Harvard Reports in Meteorology and Oceanography, Vol. 22, 31 pp.

Robinson, Allan R., Leonard J. Walstad, 1987b. "Altimetric Data Assimilation for Ocean Dynamics and Forecasting." Johns Hopkins APL Technical Digest, 8:2:267-271.

Robinson, Allan R., Michael A. Spall, Nadia Pinardi, 1988. "Gulf Stream Simulations and the Dynamics of Ring and Meander Processes." Journal of Physical Oceanography, 18:12:1811-1853.

Robinson, Allan R., Scott M. Glenn, Michael A. Spall, Leonard J. Walstad, Geraldine M. Gardner, Wayne G. Leslie, 1989. "Forecasting Gulf Stream Meanders and Rings." The Oceanography Report, 70:45:7: 3, 12-13.

Sabins, Floyd F., 1987. Remote Sensing Principles and Interpretation, New York: W. H. Freeman and Company, 449 pp.

Stommel, Henry, 1965. The Gulf Stream - A Physical and Dynamical Description, Berkeley: University of California Press, 236 pp.

Szczechowski, Carl, 1992. "Comparison of Satellite-Derived Gulf Stream Front and Eddy Analyses with GEOSAT Underflight AXBT Data." MTS Journal, 26:2:53-62.

U. S. Army Corps of Engineers, 1991. GRASS: Geographic Resource Analysis Support System, Version 4.0, Champaign, Illinois, U. S. Army Corps of Engineers.

Appendix C: Database Location and Description

The entire database constructed for this thesis was assembled on a SUN Sparcstation 2 currently located at the Institute of Marine and Coastal Sciences at Rutgers University. The data were analyzed using the Geographic Resource Analysis

Support System (GRASS) Geographic Information System. The database consisted of multiplatform satellite and in situ data collected in the Gulf Stream Meander and Ring Region during the late 1980s. This was the most data rich time period in the history of Gulf Stream observation. Specific data included Advanced Very High Resolution Radiometer images calibrated for sea surface temperature, Geosat altimeter measurements of sea surface height, and expendable bathythermograph measurements of the temperature at a 200 meter depth.

The AVHRR imagery was acquired, rectified, and converted to sea surface temperature images by the Naval Ocean Research and Development Activity (NORDA). The images are 1024 x 1024 pixels with a cell resolution of 2.25 kilometers. The temperature range of the imagery is from 5.0^{o}C to 30.5^{o}C and measured in incriments of 0.1^{o}C. All images were imported into GRASS and given color schemes using the GRASS function r.support.

The Geosat data were acquired from the National Oceanographic and Atmospheric Administration (NOAA), and had the Glenn et al. (1991a) geoid removed. The data were put into GRASS vector format by a simple Fortran program, and displayed as two lines. The Geosat track and geoid were represented by a straight line. The ocean height signal was plotted as the perpendicular offset to this straight line, with a 1 meter offset in ocean height equaling a 100 kilometer distance on the maps.

Expendable bathythermograph data were acquired from multiple sources (Table 1). All data were converted into ASCII listings of latitude, longitude, and the temperature at a 200 meter depth. The data were converted to GRASS site file format (longitude, latitude, temperature) by a Fortran program. Once in GRASS, the data were separated into 4 categories based on the temperatures at 200 meters:

1) >17.5^{o}C

2) 15-17.5°C

3) 12.5-15.0°C

4) <12.5°C

At 200 meters the 15°C isotherm is the location of the Gulf Stream north wall and warm ring edges (Cornillion and Watts, 1987).

All north wall and ring locations were digitized on screen in the GRASS program v.digit, based on enhanced and enlarged imagery, Geosat data and XBT data. The north wall lines were then smoothed using a least squares finite element cubic spline developed at Harvard University for smoothing hand digitized Gulf Stream north walls.